Summer 8-2015

Study of Surface Plasmon Resonance in Metal and Alloy Nanofilms using Maxwell Description and Metamaterial Simulation in COMSOL

Heesoo Park

Study of Surface Plasmon Resonance in Metal and Alloy Nanofilms using Maxwell Description and Metamaterial Simulation in COMSOL

A Thesis

Submitted to the Faculty

of

Rose-Hulman Institute of Technology

by

Heesoo Park

In Partial Fulfillment of the Requirements for the Degree

Of

Master of Science in Optical Engineering

August 2015

ROSE-HULMAN INSTITUTE OF TECHNOLOGY

Final Examination Report

Heesoo Park

Optical Engineering

Name

Graduate Major

Thesis Title Study of Surface Plasmon Resonance in Metal and Alloy Nanofilms using Maxell

Description and Metamaterial Simulation of COMSOL

DATE OF EXAM: August 21, 2015

EXAMINATION COMMITTEE:

	Thesis Advisory Committee	Department
Thesis Advisor:	Azad Siamakoun	PHOE
	Michael McInerney	PHOE
	Sergio Granieri	PHOE

PASSED _____X_____   **FAILED** _____

ABSTRACT

Park, Heesoo

M.S.O.E

Rose-Hulman Institute of Technology

August 2015

Study of Surface Plasmon Resonance in Metal and Alloy Nanofilms using

Maxwell Description and Metamaterial Simulation in COMSOL

Thesis Advisor: Dr. Siahmakoun Azad

Metamaterials are artificial metallic structures having, possibly, simultaneously negative permittivity and negative permeability which is called a double negative medium. To achieve a visible light range of the metamaterial, the unit cell of the metamaterial units should be 10-200nm. It is a much bigger structure than a size of normal atom. Still, the resolution of fabrication, which is difficult part, should typically be a few nanometers to achieve a nano-level unit.

We study Ag thin-film as a convenient candidate for metamaterial over a specific frequency range. Because, the thin film metal is composed of disk shape island structures itself. These represent be each metamaterial unit cell. To model the metamaterial model for each thickness of silver, we use surface plasmon-polaritons which is called SPPs. It can coupled Prism and metal to check where is

plasmon resonance angle. This specific angle and the reflectivity of a thin silver film are function of metal and dielectric of thickness and metal's permittivity and dielectric function of layer. Experimental measurements of SPPs and Simon's simulation show good agreement with the COMSOL Multiphysics metamaterial model. And we demonstrate the annealing method for a thin film metal is nice approach to change the surface plasmon resonance angle. The theory of SPPs is explained using the Drude model and Maxwell equation.

ACKNOWLEDGEMENT

I would like to thank my advisor, Professor Siahmakoun Azad, for the support and guidance he provided in the study of this topic while pursuing my master's degree. It was truly an honor for me. When I was stuck on an obstacle, your insight and enthusiasm was very helpful to me. I appreciate that you have always given me courage to pursue my career. I would also like to thank Professor Joo, Professor Granieri and Professor Mclnerney. They have given me a lot of optics knowledge. And I have really enjoyed their lectures during my master's course work.

I would like to offer thanks to my friend and colleague, Benjamin Hall, for helping my college life in the United States, and for his dedication while we worked together. His honesty and insight was very helpful to me. And I have always enjoyed communication with him.

Finally, I would like to thank my family and girlfriend for their support and encouragement. I could not have finished my thesis project if they did not support me.

TABLE OF CONTENTS

LIST OF FIGURES

LIST OF TABLES

LIST OF abbreviations

CSRR	Complimentary Split Ring Resonator
LSPR	Localized Surface plasmon resonance
DNG	Double negative medium
SE	Spectroscopic Ellipsometry
SRR	Split ring resonator
STD	Standard deviation
SPR	Surface plasmon resonance
SPP	Surface plasmon polariton
PSD	Phase Sensitive Detector
PVD	Physical Vapour Deposition

LIST OF SYMBOLS

Mathematical Symbols

B Magnetic flux density

D   Electric flux density

E   Electric field

N   The number of electrons

J   Current density

Greek Symbols

ε Permittivity

ε_m Permittivity of the metal

ε_d Permittivity of the dielectric material

ε_r Relative permittivity

μ Permeability

μ_r	Relative permeability
λ	Wavelength of light source
ω_0	Electric resonance frequency
ω_{pe}	Electric plasma frequency
ω_{pm}	Magnetic plasma frequency
θ_p	Plasmon resonance angle
ρ	Charge density

English Symbols

C	Capacitance
L	Inductance
n	Index of refraction
r	Displacement

1. Introduction

1.1 What is Surface plasmon resonance?

The surface plasmon resonance was observed by Wood in 1902. Wood observed a pattern of anomalous dark band in the reflected light[1] and Otto complete explanation of the phenomenon of surface plasmon in 1968[2]. In the same year, Kretchmann also reported the excitation of surface plasmons.

In physics, a Plasmon is quantized oscillations of free electrons. Plasmons can be described in the classical picture as an oscillation of free electron density with respect to the fixed positive ions in a metal. Plasmon can couple to the photon and create another quasiparticle called plasmon polariton, usually at the interface between metals and dielectrics. These collective oscillations of the free electrons in the metal make up dispersive longitudinal waves that propagate along the interface and decay exponentially into both dielectric medium and metal mediums with a decay length of a few tens of nanometers in the metal and up to several hundreds of nanometers in the dielectric.

As shown in Figure 1, Localized surface plasmon-resonance(LSPR) are the non propagating counterpart of surface plasmon Resonance(SPR) and is excited by a homogeneous electromagnetic wave. When the particle size of metal sphere is much smaller than the wavelength, the quasistatic approximation is

adopted in this case which means, the electric field over the nano particle can be assumed to be constant. And the field inside the particle is homogeneous and is related to the E-field.
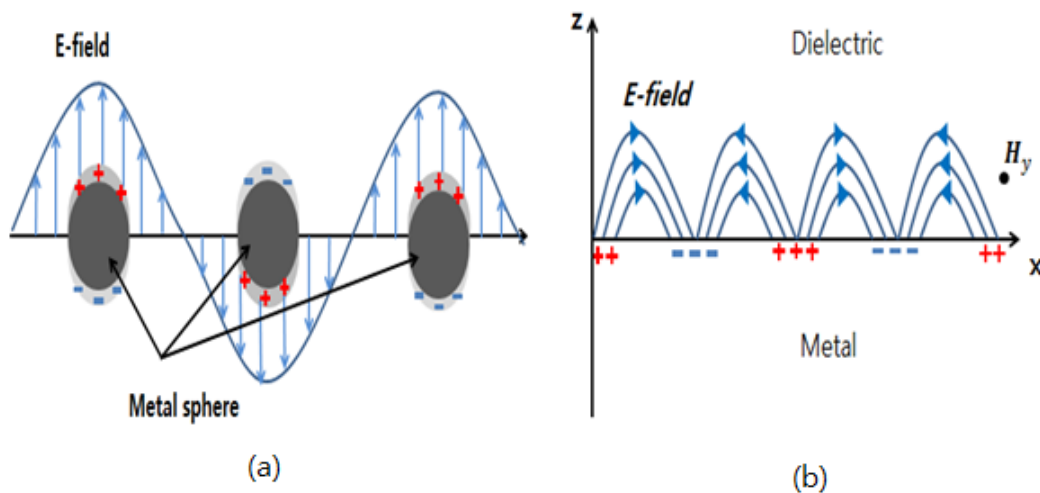
Figure 1 Schematic of Surface Plasmon Resonances (a) Localized surface plasmon: The dipole polarizability of a spherical metal nanoparticle in Electric Field (b) Charge density oscillations at the dielectric and metal interface in Electro-magnetic field

Under certain conditions, light incident on such a surface can couple to this plasmon mode to create propagating surface plasmons, also known as polarities. Excitation of surface plasmons is based on total internal reflection when an incident beam of the TM-polarized light strikes an electrically conducting metal layer at the interface of a glass prism with high refractive index and an external medium with low refractive index. At a certain angle, the excitation of surface plasmons occurs as a form of reduced intensity of the

reflected light. A surface plasmon is an electro-magnetic wave propagating along the surface of a thin film metal layer which is typically 30-80nm. Optical excitation of the surface plasmon can be achieved in the so-called Kretschmann configuration which is one of the type of SPR configuration. There are several types of SPR like Otto configuration which have this air gap between prism and a metal layer and Grating configuration as shown in Figure 2.

The angle of SPR is very sensitive to any change in the refractive index of the medium of the dielectric layer. This change is so large and have a valley intensity curve when It is at the angle of resonance. Because of this sensitivity this phenomena are used to use as a sensor for bio-sensor[3][4][5] and chemical sensor[6]and fiber optic sensor[7].

Basically, surface plasma wave is a solution of Maxwell's equation which describes how electric and magnetic fields are generated and altered by each other and by charges and currents. The specific idea of surface plasma wave is introduced in the next chapter. And we will discuss about Simon's simulation of surface plasmon excitation.
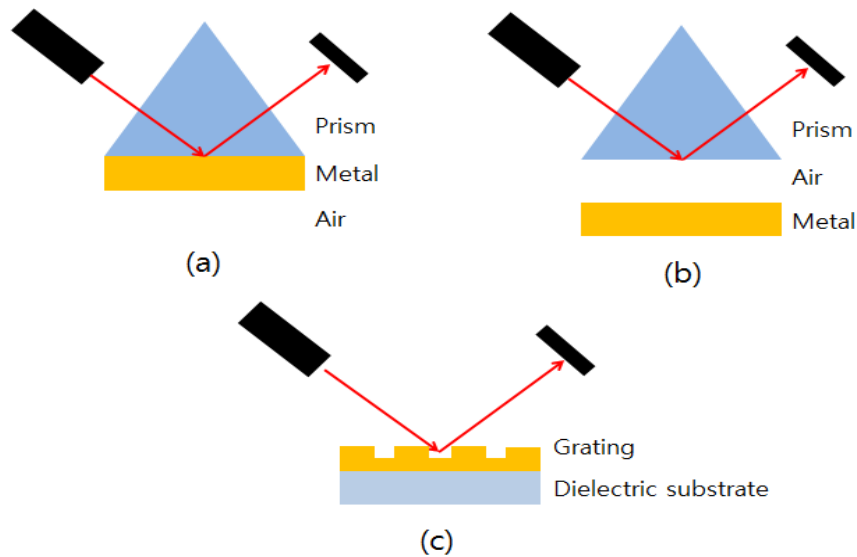
Figure 2 Surface Plasmon-Polariton Configuration. (a) Kretchmann Configuration (b) Otto Configiration (c) Grating Configuration

1.2 What is the Metamaterial?

In 1968, Russian theorist Victor Veselgo propose the concept of a medium having simultaneously negative permittivity and permeability. In his article, Veselago stated that the medium was allowed by Maxwell equations, but there is no material in nature. After almost 20 years later, Professor Pendry at Imperial College demonstrated the first non-ferrite negative permeability Metamaterial based on split ring resonators which is called SRR[8].

In an electromagnetic field, the way we can define and understand materials is based on permittivity ε and permeability μ. These properties describe how the material interacts with ElectroMagnetic light. The Permittivity

is a measure of how the applied electric field interacts with the medium and the permeability measures the response of a material to an applied magnetic field.

As shown in Figure 3. We can divide the material based on the sign of real number of permittivity and real number of permeability. Most natural materials have a positive real number of permittivity and the real number of permeability. That means most natural materials are I part in Figure 3. The materials, which has a negative real number of permittivity and positive real number of permeability is in II part.

In this part, there is the most metal and doped semiconductor. The materials, which has a negative real number of permittivity and the real number of permeability is called as Double negative medium or Metamaterial which doesn't exist in nature. The last part in Figure 3 is artificially magnetic material. And there are some ferrite materials.
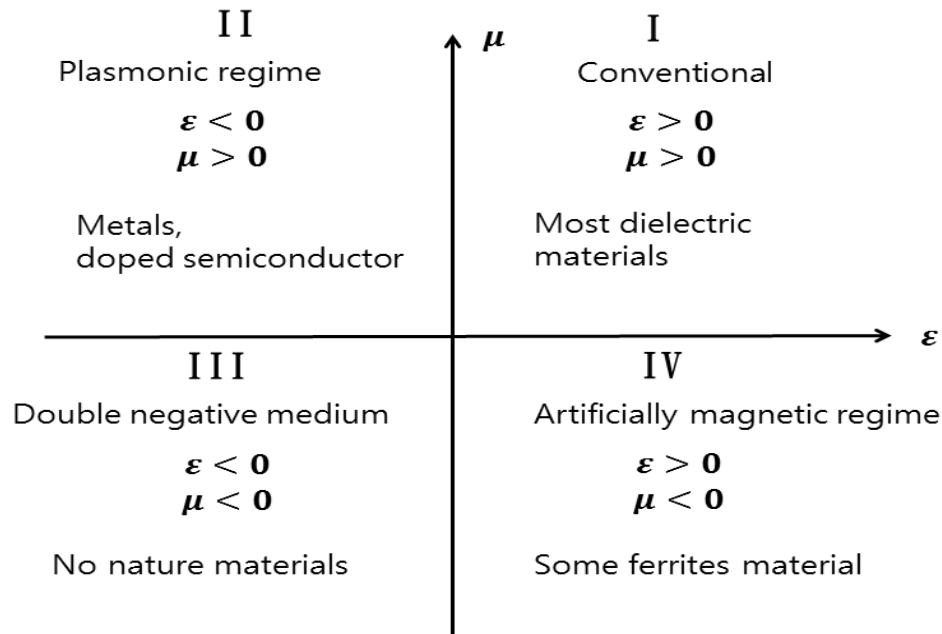
Figure 3   All materials can be characterized by their real number of permittivity and real number of permeability (I) Most dielectric materials which is real number of permittivity and real permeability is both positive   (II) The Plasmonic regime which has negative real number of permittivity and positive real number of permeability (III) Double Negative medium which is real number of permittivity and real number of permeability is both negative (IV) The aitificially magnetic regime which has positive real number of permittivity and negative real number of permeability

Metamaterials are artificial metallic structures having simultaneously negative permittivity and negative permeability which is called Double Negative medium(DNG). This DNG medium has several features that any natural medium doesn't have negative refraction, evanescent wave amplification, backward phase as a result of these, Metamaterial doesn't obey Snell's law, Doppler effect and so on. Due to this unique character of Metamaterial the concept of making a perfect lens with metamaterials has attracted attention in these days. Also miniaturization

in the size of the component is possible as the structural cell size of Metamaterial can be less than one-fourth of the guided wavelength[9]. These characters lead to solution low gain and efficiency of ordinary antenna. These can be very useful in the field of wireless communication industry.

When metals are close to its plasma frequency, the real part of the permittivity is negative. And the metal's plasma frequency is usually close to Ultraviolet frequency which is very high. But when the incident's frequency close to the metal's plasma frequency ω_p, permeability is not negative. That was the problem of the concept of Metamaterial. But Pendry introduced a periodic array of non-magnetic conducting units which is split ring resonators (SRR)[8]. He found that the SRR has an effective permeability as a function of frequencies. The SRR shape of Metal can have a negative permeability near the high resonant frequency and a negative permittivity. So SRR can be the perfect model for Metamaterial. Other researchers also found that Complementary split ring resonator (CSRR)[10], Jerusalem cross [11] and fishnet structure [12] as shown in Figure 4.
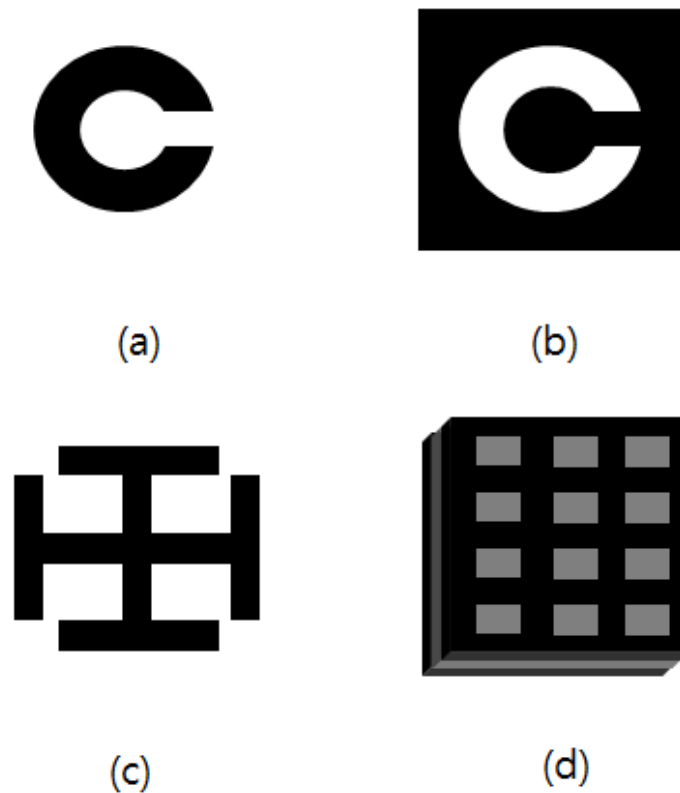
Figure 4   Various Metamaterial Type   (a) Split ring resonator (SRR)   (b) Complimentary split ring resonator(CSRR)   (c) Jerusalem cross   (d) Fishnet

The Complementary split ring resonator (CSRR) is a dual structure of SRR. That means when SRR has a metal surface as a ring resonator, The CSRR has a hole in a same space. Because of this, SRR and CSRR has a same frequency resonance theoretically, but when SRR has a bandpass filter at a specific frequency, CSRR has a band-block filter at a same frequency. This duality principle is often referred to as Baninet's principle.

The one thing that makes sure in this point is Metamaterial is not a 'new' material. Typically, When a scientist makes new material, they use chemistry for creating material. As you know, The Chemistry is the way to create material. But This is not the only way. We can artificially structure a new material by assembling an array of unit. We can call this as a Metamaterial, because this has properties that extend beyond materials which can be found in nature. Metamaterial consists of array units like SRR, Jerusalem cross and Fishnet and These each unit can act like atom to electro-magnetic wave which is significantly larger than unit size. Thus, it makes a high degree of miniaturization.

$$P < \frac{\lambda_g}{4} \qquad (1\text{-}1)$$

Where, P is the structural unit size of Metamaterial, λ_g is Guided wavelength. When electromagnetic wave incidents on a Metamaterial, the energy inside of wave affects the material's electron. This exchange of energy can be used to control electromagnetic waves. To acquire a negative index material, the plasmonic waveguides are used. These waveguides consist of thin film metal film and dielectric layer. These two material's character produces a coupled surface plasmon-polaritons(SPP).

Light incident on such a waveguide excites surface plasmon-polaritons, which excite along the waveguide on the surface of metal. The SPP can be controlled by changing metal layer's thickness and dielectric layer's thickness and by using different metals and dielectric type[13]. We described the

metamaterial on the artificial magnetic response that can be induced in several

types of metamaterials. Even though there are several designs of metamaterials,

the SRR is one of the best designs which can be easily understood. We can easily

imagine the effective capacitance C and inductance L in the SRR as shown in

Figure 5.
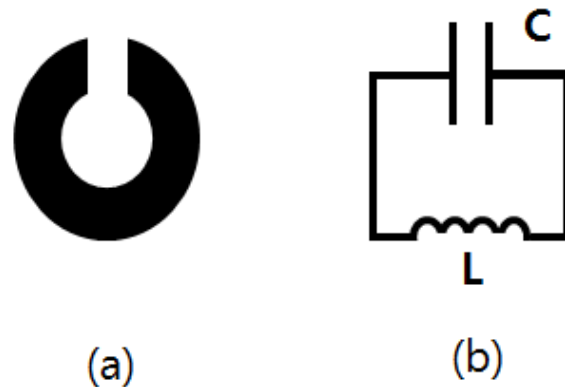
Figure 5   Split ring resonator metamaterial and it's equivalent circuit   (a) SRR(split ring resonator)   (b) Effective capacitance and inductance of SRR

The surface of the metal part of the SRR itself has an inductance in the

effective circuit. The gap of SRR has a huge portion of total effective capacitance

in the effective circuit. However, if the SRR unit is close enough to the other

SRR unit, that part of the calculation should be considered as another

capacitance. The split ring resonator is an element capable of achieving strong

magnetism.

1.3 Thesis scope

Electo-magnetic radiation incident on a metamaterial excites surface plasmon polaritons.[14,15] Surface plasmon resonance can be altered by the dielectric and metal material of permittivities. The reflectivity depends on angle difference, and is a function of surface plasmon resonance and of the thickness og the metal.

In this thesis, We're going to deal with thin silver layer and evaluate the surface plasmon resonance at thicknesses of 17nm, 35nm, 57nm of Ag layer. To observe surface plasmon resonance in Ag, a magnetron sputtering system is used for deposition of Ag. The thickness of Ag was measured by Stylus Profiler and each Ag layer was characterized by an Elipsometer. After we generated a surface plasmon resonance graph depends on the incident angle, the equivalent metamaterial model was found with COMSOL Multiphysics. The disk type metamaterials simulation using COMSOL Multiphysics is compared with the SPR result for each thickness of Ag. The annealing method is presented to change the surface plasmon resonance angle.

2. Theory

2.1 Maxwell model for surface plasmon resonance

Maxwell's equations describe how electric and magnetic fields are generated and altered by each other and by charges and currents. This fits well with surface plasmon resonance(SPR). To do describe SPR, We can start with Maxwell equations.

$$\nabla \cdot \mathbf{D} = \rho_V \qquad (\,2\text{-}1)$$

$$\nabla \cdot \mathbf{B} = 0 \qquad (2\text{-}2)$$

$$\nabla \times \mathbf{E} = -\frac{\partial \mathbf{B}}{\partial t} \qquad (2\text{-}3)$$

$$\nabla \times \mathbf{H} = \frac{\partial \mathbf{D}}{\partial t} + \mathbf{J} \qquad (2\text{-}4)$$

In a homogeneous and isotropic medium, with charge density $\rho = 0$ and current density $\vec{J}=0$, the dielectric permittivity ε and the magnetic permeability μ can be assumed to be scalar. The polarization of the material and an associated electric field can be written $\vec{B} = \mu_r \mu_0 \vec{H}$ and $\vec{D} = \varepsilon_r \varepsilon_0 \vec{E}$, respectively.

$$\nabla \cdot \mathbf{E} = 0 \qquad (2\text{-}5)$$

$$\nabla \cdot \mathbf{H} = 0 \qquad (2\text{-}6)$$

$$\nabla \times \mathbf{E} = -j\omega \mu_r \mu_0 \mathbf{E} \qquad (2\text{-}7)$$

$$\nabla \times \mathbf{H} = \mathrm{j}\omega\varepsilon_r\varepsilon_0\boldsymbol{H} \qquad\qquad (2\text{-}8)$$

For 1-Dimension geometries, we have a uniform material in the y-direction as shown in Figure 6. Maxwell's equations can be divided into two independent modes.
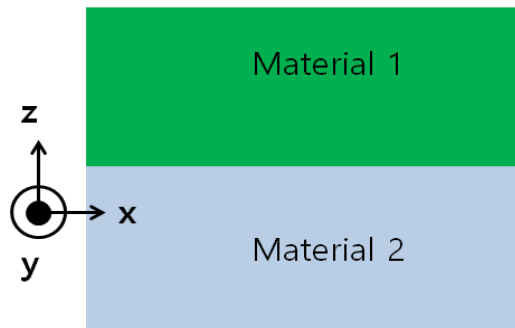
Figure 6   Model geometry and direction for SPP

$$\frac{\partial \mathbf{H}_x}{\partial z} - \frac{\partial \mathbf{H}_z}{\partial x} = \mathrm{j}\omega\varepsilon_r\varepsilon_0\boldsymbol{E}_y \qquad\qquad (2\text{-}9)$$

$$-\frac{\partial \mathbf{E}_y}{\partial z} = -\mathrm{j}\omega\mu_r\mu_0\boldsymbol{H}_x \qquad\qquad (2\text{-}10)$$

$$\frac{\partial \mathbf{E}_y}{\partial x} = -\mathrm{j}\omega\mu_r\mu_0\boldsymbol{H}_z \qquad\qquad (2\text{-}11)$$

$$\frac{\partial \mathbf{E}_x}{\partial z} - \frac{\partial \mathbf{E}_z}{\partial x} = -\mathrm{j}\omega\mu_r\mu_0\boldsymbol{H}_y \qquad\qquad (2\text{-}12)$$

$$-\frac{\partial \mathbf{H}_y}{\partial z} = \mathrm{j}\omega\varepsilon_r\varepsilon_0\boldsymbol{E}_x \qquad\qquad (2\text{-}13)$$

$$\frac{\partial \mathbf{H}_y}{\partial x} = \mathrm{j}\omega\varepsilon_r\varepsilon_0\boldsymbol{E}_z \qquad\qquad (2\text{-}14)$$

In Figure 6, the lower material is a metal. A plane boundary exists between the two areas, as is shown in Figure 6. The dielectric constant of medium 1 is assumed to be real and positive. If a surface wave is to propagate along the surface of a metal, these waves propagate along the surface z=0. We can choose any x and y orientation of our coordinate system, so a set of waves is chosen that has no y-component. We can thus ignore the first set of equations to simplify the calculation.

If the wave is a surface wave, it must be confined to the surface. This implies the field solution will assume the following form.

$$\mathbf{E}_{i(z)} = \begin{bmatrix} E_{x,i} \\ E_{z,i} \end{bmatrix} e^{-K_i|x|} e^{-j\beta z} \tag{2-15}$$

$$\mathbf{H}_{i(z)} = H_{y,i} e^{-K_i|x|} e^{j\beta z} \tag{2-16}$$

$$i = \begin{cases} 1, & x < 0 \\ 2, & x > 0 \end{cases}$$

This assumed solution yields the following equation.

$$\frac{\partial}{\partial z}\left(E_{x,i} e^{-K_i|x|} e^{-j\beta z}\right) - \frac{\partial}{\partial x}\left(E_{z,i} e^{-K_i|x|} e^{-j\beta z}\right) =$$

$$-j\omega\mu_{r,i}\mu_0\left(H_{y,i} e^{-K_i|x|} e^{j\beta z}\right) \tag{2-17}$$

$$-\frac{\partial}{\partial z}\left(H_{y,i} e^{-K_i|x|} e^{j\beta z}\right) = j\omega\varepsilon_{r,i}\varepsilon_0\left(E_{x,i} e^{-K_i|x|} e^{-j\beta z}\right) \tag{2-18}$$

$$\frac{\partial}{\partial x}\left(H_{y,i} e^{-K_i|x|} e^{j\beta z}\right) = j\omega\varepsilon_{r,i}\varepsilon_0\left(E_{z,i} e^{-K_i|x|} e^{-j\beta z}\right) \tag{2-19}$$

Inside medium 1, the Eq. 2-17, 2-18, 2-19 were

$$\frac{\partial}{\partial z}\left(E_{x,1}e^{-K_1|x|}e^{-j\beta z}\right) - \frac{\partial}{\partial x}\left(E_{z,1}e^{-K_1|x|}e^{-j\beta z}\right) =$$

$$-j\omega\mu_{r,1}\mu_0\left(H_{y,1}e^{-K_1|x|}e^{j\beta z}\right) \tag{2-20}$$

$$-\frac{\partial}{\partial z}\left(H_{y,1}e^{-K_1|x|}e^{j\beta z}\right) = j\omega\varepsilon_{r,1}\varepsilon_0\left(E_{x,1}e^{-K_1|x|}e^{-j\beta z}\right) \tag{2-21}$$

$$\frac{\partial}{\partial x}\left(H_{y,1}e^{-K_1|x|}e^{j\beta z}\right) = j\omega\varepsilon_{r,1}\varepsilon_0\left(E_{z,1}e^{-K_1|x|}e^{-j\beta z}\right) \tag{2-22}$$

These reduce to the following equations.

$$j\beta E_{x,1} + K_1 E_{z,1} = -j\omega\mu_{r,1}\mu_0 H_{y,1} \tag{2-23}$$

$$-j\beta H_{y,1} = j\omega\varepsilon_{r,1}\varepsilon_0 E_{x,1} \tag{2-24}$$

$$-K_1 H_{y,1} = j\omega\varepsilon_{r,1}\varepsilon_0 E_{z,1} \tag{2-25}$$

Inside of medium 2, Above Eq. 2-17, 2-18, 2-19 were

$$\frac{\partial}{\partial z}\left(E_{x,2}e^{-K_2|x|}e^{-j\beta z}\right) - \frac{\partial}{\partial x}\left(E_{z,2}e^{-K_2|x|}e^{-j\beta z}\right) =$$

$$-j\omega\mu_{r,2}\mu_0\left(H_{y,2}e^{-K_2|x|}e^{j\beta z}\right) \tag{2-26}$$

$$-\frac{\partial}{\partial z}\left(H_{y,2}e^{-K_2|x|}e^{j\beta z}\right) = j\omega\varepsilon_{r,2}\varepsilon_0\left(E_{x,2}e^{-K_2|x|}e^{-j\beta z}\right) \tag{2-27}$$

$$\frac{\partial}{\partial x}\left(H_{y,2}e^{-K_2|x|}e^{j\beta z}\right) = j\omega\varepsilon_{r,2}\varepsilon_0\left(E_{z,2}e^{-K_2|x|}e^{-j\beta z}\right) \tag{2-28}$$

These equations reduce to the following equations.

$$j\beta E_{x,2} + K_2 E_{z,2} = -j\omega\mu_{r,2}\mu_0 H_{y,2} \tag{2-29}$$

$$-j\beta H_{y,2} = j\omega\varepsilon_{r,2}\varepsilon_0 E_{x,2} \tag{2-30}$$

$$-K_2 H_{y,2} = j\omega\varepsilon_{r,2}\varepsilon_0 E_{z,2} \tag{2-31}$$

The field component $\mathbf{E}_x$ which is longitudinal to this interface is eliminated from the above Eq. 2-23, 2-24, 2-25, 2-26, 2-27, 2-28 to match the boundary conditions. At Medium 1,

$$K_1 E_{z,1} = \frac{-j}{\omega \varepsilon_{r,1} \varepsilon_0}(k_0{}^2 \mu_{r,1} \varepsilon_{r,1} - \beta^2) H_{y,1} \tag{2-32}$$

$$K_1 H_{y,1} = -j\omega \varepsilon_{r,1} \varepsilon_0 E_{z,1} \tag{2-33}$$

At Medium 2,

$$K_2 E_{z,2} = \frac{j}{\omega \varepsilon_{r,2} \varepsilon_0}(k_0{}^2 \mu_{r,2} \varepsilon_{r,2} - \beta^2) H_{y,2} \tag{2-34}$$

$$K_2 H_{y,2} = j\omega \varepsilon_{r,2} \varepsilon_0 E_{z,2} \tag{2-35}$$

There are no more $\mathbf{E}_x$ components in among Eq. 2-32, 2-33, 2-34, 2-35. The dispersion relations is derived by further eliminating Ez, and results in a relation with remaining parameters.

$$k_0{}^2 \mu_{r,i} \varepsilon_{r,i} = \beta^2 - K_i{}^2 \tag{2-36}$$

At each medium,

$$k_0{}^2 \mu_{r,1} \varepsilon_{r,1} = \beta^2 - K_1{}^2 \tag{2-37}$$

$$k_0{}^2 \mu_{r,2} \varepsilon_{r,2} = \beta^2 - K_2{}^2 \tag{2-38}$$

As electric field boundary conditions $E_{z,1} = E_{z,2}$

$$\frac{-j}{\omega \varepsilon_{r,1} \varepsilon_0 K_1}(k_0{}^2 \mu_{r,1} \varepsilon_{r,1} - \beta^2) H_{y,1} = \frac{j}{\omega \varepsilon_{r,2} \varepsilon_0 K_2}(k_0{}^2 \mu_{r,2} \varepsilon_{r,2} - \beta^2) H_{y,2}$$

$$\tag{2-39}$$

$$\frac{K_1}{\varepsilon_{r,1}} + \frac{K_2}{\varepsilon_{r,2}} = 0 \tag{2-40}$$

As a magnetic field boundary conditions $H_{y,1} = H_{y,2}$

$$\frac{-j\omega\varepsilon_{r,1}\varepsilon_0}{K_1}E_{z,1} = \frac{j\omega\varepsilon_{r,2}\varepsilon_0}{K_2}E_{z,2} \tag{2-41}$$

$$\frac{\varepsilon_{r,1}}{K_1} + \frac{\varepsilon_{r,2}}{K_2} = 0 \tag{2-42}$$

The equation of boundary conditions and Eq. 2-37, Eq. 2-28 relation is used by eliminating the K terms.

$$\beta^2 = k_0{}^2\left(\frac{1}{\varepsilon_{r,1}{}^2} - \frac{1}{\varepsilon_{r,2}{}^2}\right)^{-1}\left(\frac{\mu_{r,1}}{\varepsilon_{r,1}} - \frac{\mu_{r,2}}{\varepsilon_{r,2}}\right) \tag{2-43}$$

For non-magnetic materials with $\mu_{r,i} = 0$, Eq. 2-43 is reduced to the following equation.

$$\beta = k_0\sqrt{\frac{\varepsilon_{r,1}\varepsilon_{r,2}}{\varepsilon_{r,1}+\varepsilon_{r,2}}} \tag{2-44}$$

The dispersion relation can expressed like the following equation also.

$$k = \frac{2\pi}{\lambda}\sqrt{\frac{\varepsilon_m\varepsilon_d}{\varepsilon_m+\varepsilon_d}} \tag{2-45}$$

Here, λ is the wavelength of the excitation wave, ε_m is the complex dielectric function of the metal and ε_d is the dielectric function of the surrounding material. An evanescent wave can exist at the angle of total internal reflection which means that beyond the critical angle of material passes to the metal and extinguishes at a shallow depth. When the metal layer is thin enough, this wave can interact with the surface charges, and then an energy transfer occures from the excitation wave to the plasmon wave. This effect is called the plasmon effect. We can detect this wave when the reflected light wave parallel to the surface is equal to the plasmon wave vector.

$$k_{light} = k_{plasmon} \tag{2-46}$$

$$\frac{2\pi}{\lambda} n \sin\theta = \frac{2\pi}{\lambda} \sqrt{\frac{\varepsilon_m \varepsilon_d}{\varepsilon_m + \varepsilon_d}} \tag{2-47}$$

Here, θ is the angle of the light reflection of the surface and, n is the index of refraction for the dielectric material which is prism in this case. In order to describe the plasmon angle we employ, the following equation.

$$\theta_p = \sin^{-1}\left(n^{-1}\sqrt{\frac{\varepsilon_m \varepsilon_d}{\varepsilon_m + \varepsilon_d}}\right) \tag{2-48}$$

In this study, we use silver, which has a negative real component to its dielectric constant and a very low imaginary part. And θ_p is the key element to compare between real metal layer's plasmon effect and COMSOL equivalent model.

The amplitude of the surface plasmon mode is related to the exciting incident radiation. An electromagnetic light in a prism is incident on a thin film metal layer. We assume the electric field is TM mode and composed of monochromatic plane waves. The following equations are the incident and reflected propagating wave of the form in the prism. The attenuated total incident and reflection geometry is shown in Figure 7.
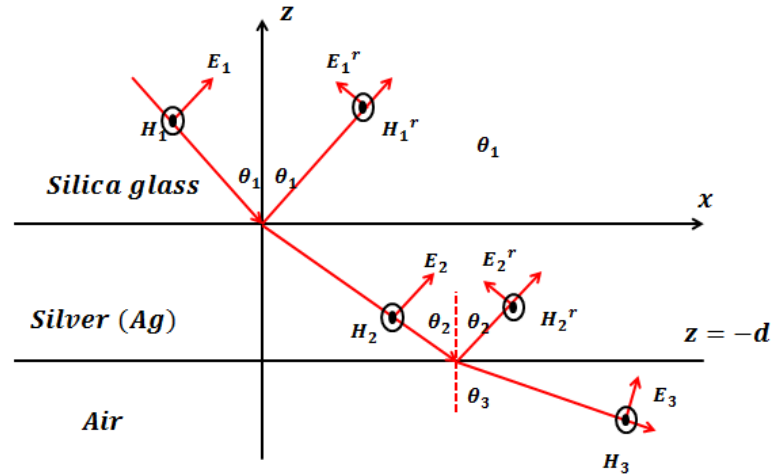
Figure 7   Attenuated total incident and reflection geometry for a thin metal layer between silica glass and air.

$$E_i = E_1 e^{[i\left(\frac{n\omega}{c}\right)(x \sin \theta_1 - z \cos \theta_1)]} \tag{2-49}$$

$$E_r = E_1{}^r e^{[i\left(\frac{n\omega}{c}\right)(x \sin \theta_1 + z \cos \theta_1)]} \tag{2-50}$$

In a thin film metal layer, the total electric field is considered as a standing wave superposition of two exponentially damped waves. And the transmitted wave in the air is assumed to be evanescent.

$$E_m = E_2 e^{[i\left(\frac{n\omega}{c}\right)(x \sin \theta_1)]} e^{(kz)} + E_2{}^r e^{[i\left(\frac{n\omega}{c}\right)(x \sin \theta_1)]} e^{(-kz)} \tag{2-51}$$

$$E_t = E_3 e^{[i\left(\frac{n\omega}{c}\right)(x \sin \theta_1)]} e^{[z\left(\frac{\omega}{c}\right)(n^2 (\sin \theta_1)^2)^{1/2}]} e^{(-kz)} \tag{2-52}$$

A single wave on each side of the boundary exists. The electric field is assumed to be a monochromatic plane wave. In wave propagation in an infinite solid, k_x, k_z are to be given real numbers and the wave equation is used to determine the frequency of the propagating wave. With these conditions, there

are no propagating waves in either the metal and air. And ω and k_x are assumed to values that satisfy the wave equation in the following form within the metal.

$$E(x, z, t) = Ee^{[i(\omega t - k_x x - k_z z)]} \tag{2-53}$$

$$k_x = -i(k_x{}^2 - \frac{\varepsilon \omega^2}{c^2})^{1/2} \tag{2-54}$$

The above equations, can be written like this.

$$k = -i(\frac{\omega}{c})(\varepsilon - n^2 \sin \theta_1{}^2)^{1/2} \tag{2-55}$$

Here, ε is the complex dielectric coefficient of the metal, n is the index of refraction of the prism, and θ_1 is the angle of incidence between Prism and metal.

As shown in Figure 7, the boundary condition, which dictates the continuity of the tangential components of E and H at the z=0, z=-d boundaries yeilds the following equations.

$$E_2 = E_1 t_{12}/(1 + r_{12} r_{23} e^{-2kd}) \tag{2-56}$$

$$E_2{}^r = E_1 t_{12} r_{23} e^{-2kd}/(1 + r_{12} r_{23} e^{-2kd}) \tag{2-57}$$

With the subscript 12 represents the prism-metal interface and number 23 stands for metal-air boundaries. The Fresnel reflection and transmission amplitude factors are given by

$$t_{12} = \frac{2n \cos \theta_1}{\varepsilon^{1/2} \cos \theta_1 + n \cos \theta_2} \tag{2-58}$$

$$r_{12} = \frac{\varepsilon^{1/2} \cos \theta_1 - n \cos \theta_2}{\varepsilon^{1/2} \cos \theta_1 + n \cos \theta_2} \tag{2-59}$$

$$r_{23} = \frac{-\varepsilon^{1/2} \cos\theta_3 + \cos\theta_2}{\varepsilon^{1/2} \cos\theta_3 + \cos\theta_2} \qquad (2\text{-}60)$$

The angles θ_2 and θ_3 are defined by,

$$\cos\theta_2 = (1 - n^2 \sin\theta_1^2 / \varepsilon)^{1/2} \qquad (2\text{-}61)$$

$$\cos\theta_3 = (1 - n^2 \sin\theta_1^2)^{1/2} \qquad (2\text{-}62)$$

After solving for $E_1{}^r$, the ratio of the reflected optical power to the

incident optical power to be given by

$$\text{R} = \left[\frac{r_{12} + r_{23} e^{-2kd}}{1 + r_{12} r_{23} e^{-2kd}}\right]^2 \qquad (2\text{-}63)$$

In this study, we use this equation for simulation. [16]

2.2 Metamaterial model

The temporal response of a chosen polarization field component to the

same component of the electric field, assuming that the electric charges move to

the same direction as the electric field. We consider a case in which the electron

can occupy a location in the lattice that is an energy minimum. This can be

described by a material model called the Lorentz Model. And any energy

minimum model can be parabolic leading to Hooke's Law. And energy is

considered as a power series expansion about the minimum.

$$\text{E(r)} = E|_{r=0} + (r-0)\frac{\partial E}{\partial r}\Big|_{r=0} + \frac{(r-0)^2}{2!}\frac{\partial^2 E}{\partial r^2}\Big|_{r=0} + \cdots \qquad (2\text{-}64)$$

Here, r is displacement, and E is Energy. The first term can be eliminated by choosing zero. The second term which is the first derivative is also zero at the minimum. This is cause the value of the potential energy is at minimum. The above equation describes to following equation.

$$E(r) \cong \frac{r^2}{2!}\frac{\partial^2 E}{\partial r^2} = \frac{1}{2}kr^2 \tag{2-65}$$

The electron can be modeled as being bound by Hooke's Law. Let's assume a loss term which is proportional to the speed of the electron which is mainly loss due to scattering and associated phonon coupling, which occurs when charge collides into the lattice, causing lattice to vibrate. Then let's apply Newton's second law for the electron with mass m and charge −e, in an electric field E.

$$m\frac{d^2r}{dt^2} = -eE - kr - b\frac{dr}{dt} \tag{2-66}$$

where b is Γm, k is $m\omega_0^2$. and $\omega_0 = \sqrt{\frac{k}{m}}$. Now, apply these to the previous equation.

$$m\frac{d^2r}{dt^2} = -eE - m\omega_0^2 r - \Gamma m\frac{dr}{dt} \tag{2-67}$$

$$\frac{d^2r}{dt^2} = -\frac{e}{m}E - \omega_0^2 r - \Gamma\frac{dr}{dt} \tag{2-68}$$

$$\frac{d^2r}{dt^2} + \Gamma\frac{dr}{dt} + \omega_0^2 r = -\frac{e}{m}E \tag{2-69}$$

Now, let's adopt the frequency domain which means $\frac{d}{dt} = j\omega(i\omega)$.

$$-\omega^2 r - j\omega\Gamma r + \omega^2 r = -\frac{e}{m}E \tag{2-70}$$

$$r = \frac{-\frac{e}{m}E}{\omega_0{}^2 - \omega^2 + j\omega\Gamma} \tag{2-71}$$

$$P = Np = \frac{-\frac{Ne^2}{m}E}{\omega_0{}^2 - \omega^2 + j\omega\Gamma} \tag{2-72}$$

Let's apply $p = -er$. And P=Np, N is the number of electrons.

To describe more, we need to introduce one of Maxwell equations.

$$D = \varepsilon E = \varepsilon_0 E + (\varepsilon_r - 1)\varepsilon_0 E = \varepsilon_0 E + \chi_e \varepsilon_0 E \qquad \text{(Eq. 2-73)}$$

Here, D is electric flux Density, ε_r is relative electric permittivity, ε_0 is vacuum's electric permittivity and E is electric field. Let's apply this equation to following one.

$$\chi_e \varepsilon_0 E = P = \frac{-\frac{Ne^2}{m}E}{\omega_0{}^2 - \omega^2 + j\omega\Gamma} \tag{2-74}$$

$$\chi_e = P = \frac{-\frac{Ne^2}{\varepsilon_0 m}}{\omega_0{}^2 - \omega^2 + j\omega\Gamma} \tag{2-75}$$

$$\chi_e = \frac{-\omega_p{}^2}{\omega_0{}^2 - \omega^2 + j\omega\Gamma} \tag{2-76}$$

Here, ω_p is electric plasma frequency, ω_0 is electric resonant frequency, Γ is electric damping frequency. We describe the Lorentz model of the electron, but the study we use the Drude model which is valid for free charges, where electrons are not bound to host molecules. This decribes the environment for electrons in metals, which is considered as an electron gas. $(\omega_0 = 0)$

$$\chi_e(\omega) = \frac{-\omega_p{}^2}{-\omega^2 + j\omega\Gamma} \tag{2-77}$$

$$\varepsilon(\omega) = \varepsilon_0(1 + \chi_e) = \varepsilon_0\left(1 - \frac{\omega_p{}^2}{\omega^2 - j\omega\Gamma}\right) \tag{2-78}$$

Here, $\omega_p{}^2$ is $\frac{Ne^2}{\varepsilon_0 m}$. The plasma frequency is typically in the ultraviolet(UV) range. The damping parameter Γ is typically well into the infrared(IR) range. This means that the real part of permittivity can be real and negative for frequencies in the a near IR and above. For frequencies lower than near IR, ε becomes a largely imaginary number, which means that loss begins to dominate.

In the frequency domain, the permittivity and permeability in the Drude metamaterial model can be described by

$$\varepsilon(\omega) = \varepsilon_0(1 - \frac{\omega_{pe}{}^2}{\omega^2 - j\omega\Gamma_e}) \tag{2-79}$$

$$\mu(\omega) = \mu_0(1 - \frac{\omega_{pm}{}^2}{\omega^2 - j\omega\Gamma_m}) \tag{2-80}$$

Here, ω_{pe} is electric plasma frequency, Γ_e is electric damping frequency, ω_{pm} is magnetic plasma frequency and Γ_m is magnetic damping frequency. j is the imaginary unit. [17,18]

2.3 Thin film metal-island surface

When a thin film of metal surface was seen by bare eyes, it appears flat and semi-transparent, because the structure of thin film metal is typically less than 100nm[19]. The thin film of metal-island surface is seen when we use slow evaporation rates using Physical Vapour Deposition(PVD). The scanning electron microscope (SEM) is used to view those structures. However, when the

metal thickness is large enough, the metal layer becomes almost completely continuous. At high evaporation rates, the surface of the metal becomes more continuous.

This thin film of metal surface has a nano-island surface as shown in Figure 8.
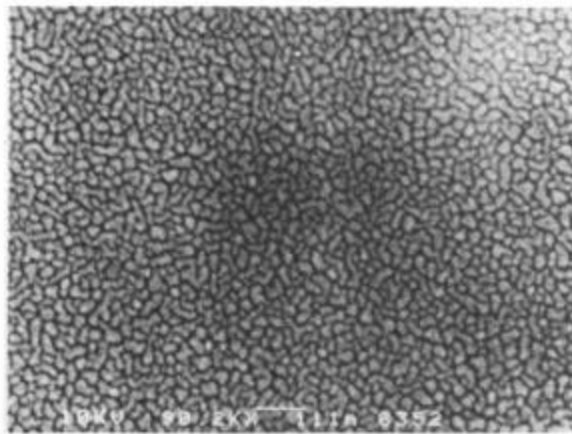
Figure 8 Scanning electron micrograph of a thin(5-nm) silver evaporation on silicon at room temperature. Bar indicates a length of 111nm[20].

Annealing the layer of metal helps to reorganize the size of nano-island, making them larger as shown in Figure 9.
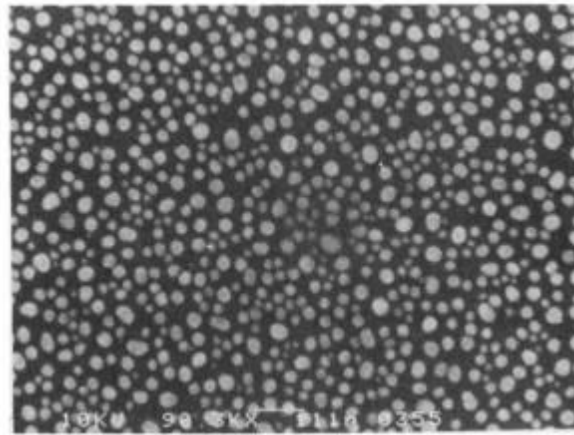
Figure 9   Evaporated silver film on silicon after a 1-min anneal at 200℃. Same scale as Fig.8 [20].

The annealing temperature, and annealing duration determine the size and organization of the silver nano-islands[20].

As shown in Figure 8, Figure 9. The thin film of metal surface has a nano – island surface. That's why the COMSOL model was constructed to resemble the disk type of nano-island surface.

2.4   COMSOL SRR

COMSOL Multiphysics 4.3 was used for simulating metamaterial. COMSOL basically follows Maxwell's equation which were described in the previous chapter, and they use finite difference methods called FEM. This means they are based on unstructured grids. FEM is more flexible with respect to the

geometry and is a numerical technique for finding approximate solutions to boundary value problems for partial differential equations. As shown in the previous chapter, metamaterials have arrays of units. In this COMSOL simulation, a split ring resonator was used and this model shows that only signals around the center frequency can pass through the periodic complimentary split ring resonator layer.

A split ring resonator is patterned on a geometrically thin Ag layer on the substrate. The metal layer is much thicker than the skin depth in the simulated frequency range, so it is modeled as a perfect electric conductor. And Floquet-periodic boundary conditions which are the solutions to periodic linear differential equations are used on four sides of the unit cell to simulate the infinite 2D array. Perfectly matched layers on the top and bottom of the unit cell absorb the excited mode from the source port and any higher order modes generated by the periodic structure. The perfectly matched layers(PML) attenuate the wave as it propagates in the direction perpendicular to the PML boundary. Port boundary conditions are placed on the interior boundaries of the PML, adjacent to the air domains. The port boundary conditions will automatically determine the reflection and transmission characteristics in terms of S-parameters. Since higher order diffraction modes are not of particular interest in this model, the combination of the domain-backed type slit port and PML is used instead of adding a diffraction order port for each diffraction order. The periodic

boundary condition requires identical surface meshes on paired boundaries by creating a mesh on only one of the boundaries and then using the copy face operation for the mesh on the other boundary.

As we described above section, The metamaterial have several shapes and types. The most popular one is SRR, which is split ring resonator, CSRR which is a complimentary split ring resonator, Jerusalem cross and Fishnet. In this study, the disk type of metamaterial is well fitted to the metal's plasma effect and Simon's model. The disk type of metamaterial is shown in Figure 10, Figure 11, which is a 2-D model. This is basically an infinite disk array toward the x-axis and y-axis. The black part of this model represents the metal part, and the white part of this model symbolizes the dielectric part which doesn't flow current. This dielectric part can be air, glass, plastic or a metal oxide layer. As shown in Figure 10, the 'a' size is same with 'b' and r stands for the radius of circle of metal or hole.

Figure 10   Disk type of Metamaterial design and dimension. 'a' and 'b' is gap between disk and 'r' stands for the radius of disk.

As shown in Figure 11, the complimentary disk type of metamaterial model has a hole in the white part of the disk, and the dark part represents the metal. The COMSOL model also has a hole in the disk part and has a metal surface in the other part as shown in Figure 12. To correctly calculate the model in COMSOL, a small mesh period was generated by mesh generator. The biggest mesh period is ten times smaller than the wavelength which is 632.8nm as shown in Figure 13. However, the memory requirement is too cumbersome to handle with available resources. COMSOL software has a periodic condition for simple periodic

sample. In this study, this model can be reduced in the other model as shown in

Figure 14, which is easier to calculate and simple.

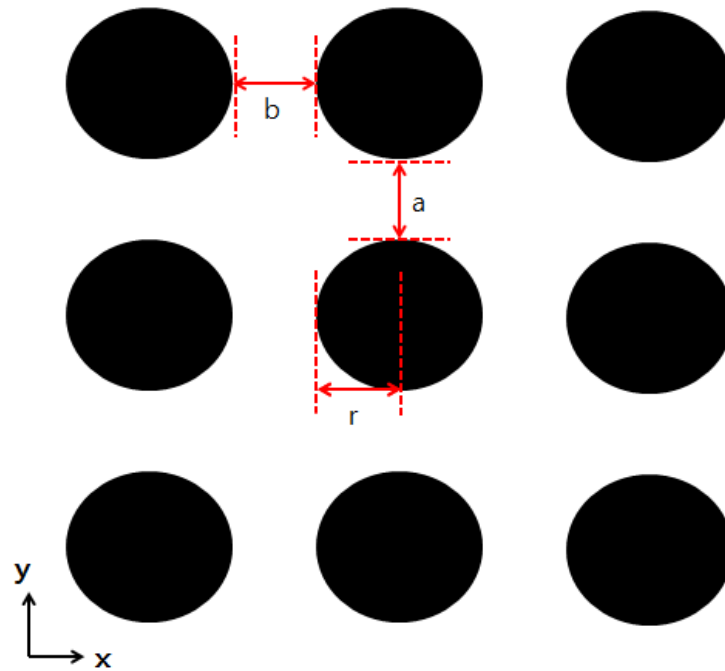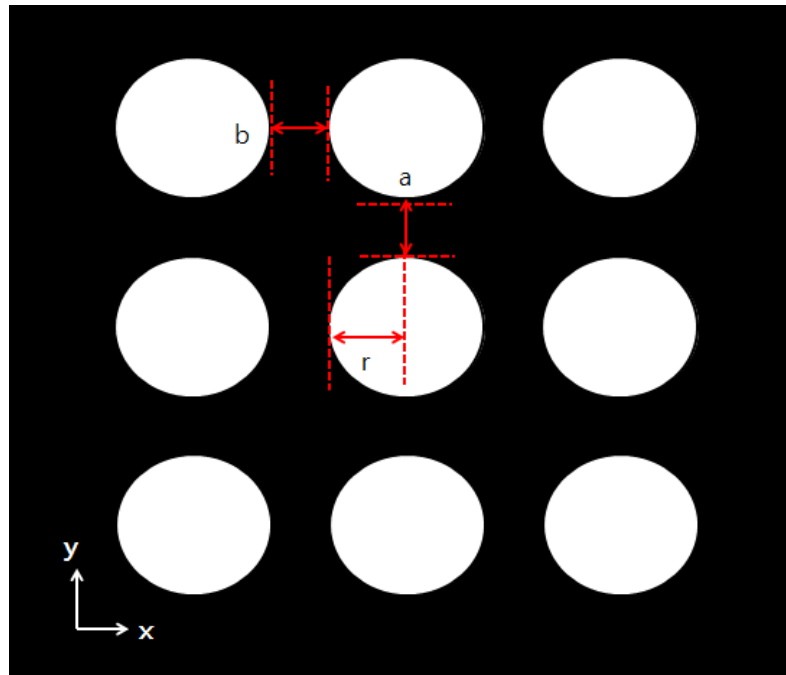**Figure 11   Complimentary disk type of metamaterial design and dimension. 'a' and 'b' is a gap between disk and 'r' stands for the radius of the disk.**
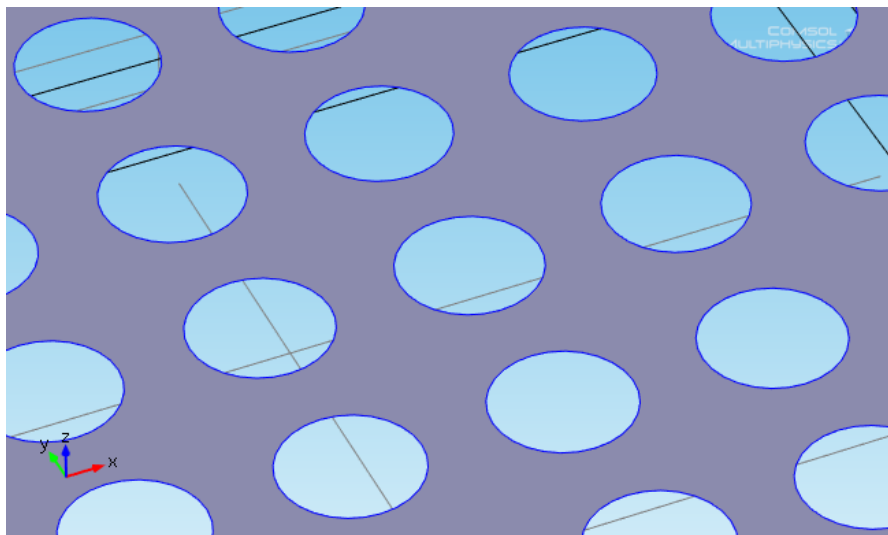
Figure 12 COMSOL model for complimentary disk type
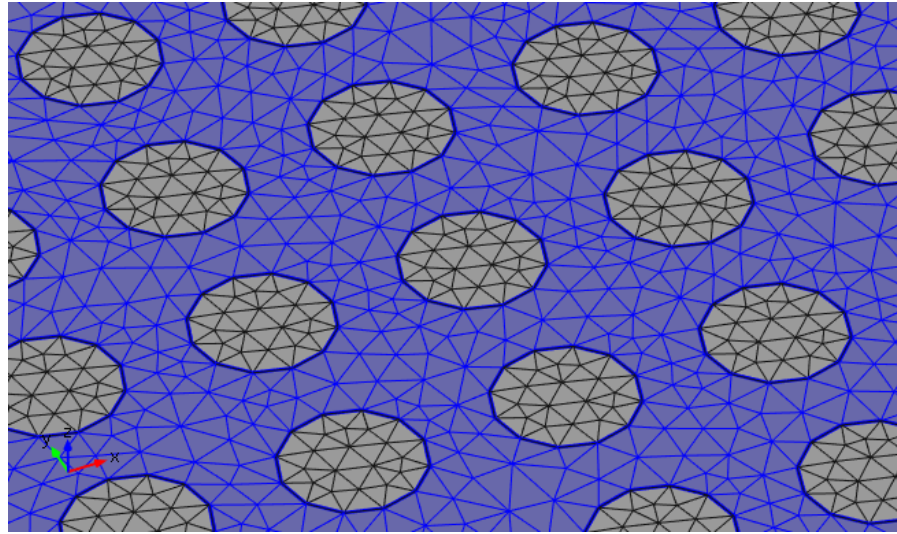
Figure 13 COMSOL mesh model for complimentary disk type
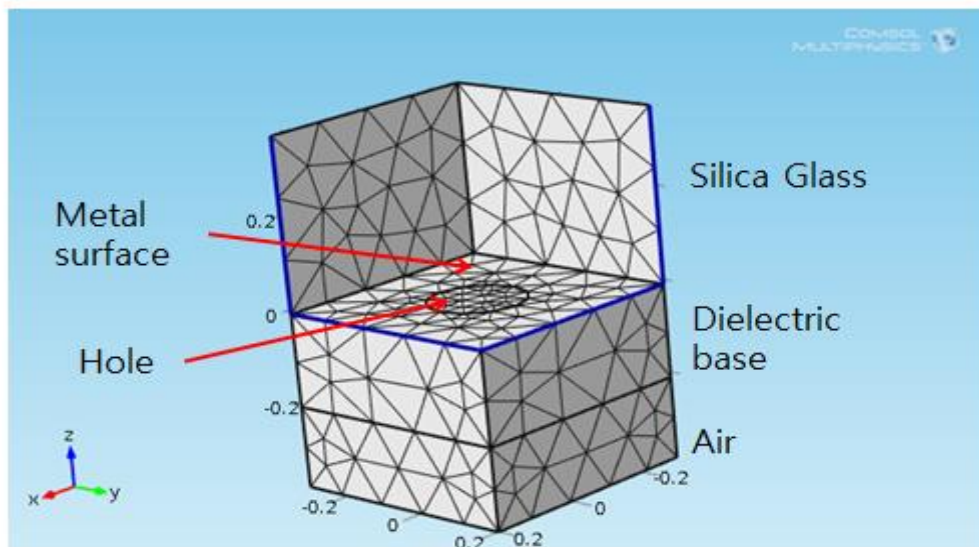
Figure 14   COMSOL model for equivalent surface plasmon polariton using disk type of metamaterial

As mentioned above, this model has an infinite array in the x and y directions. The top material is silica glass which has and index of 1.457. The

middle material is a dielectric substrate which can be plastic, glass on metal

Oxide. The Botton part is air. This COMSOL model was constructed to resemble

the plasma effect system and thin-metal nano-island model.

3. Surface plasmon resonance experiments

The He-Ne laser which is a monochromatic, TM-polarized beam of light is incident upon the silver film. The beam reflects off the silver film and generates the evanescent field inside of the silver. The evanescent field passes through the silver layer and dielectric layer, which is air, and excites a surface plasmon wave between two materials.

3.1 Fabrication thin film of metal for surface plasmon resonance

A silver film was deposited onto the hypotenuse face of a prism using a magnetron sputtering as shown in Figure 15. Magnetron sputtering is a method of physical vapour deposition(PVD), which is a plasma coating deposition technology. Magnetron sputtering is an alternative method of evaporation for metal film deposition. The method has better step coverage than evaporation and is better at producing layers of compound materials and alloys. In sputtering applications, high energy ions strike a target containing the material to be deposited. Because of the momentum exchange between the ions and the particles in the target, the material is ejected from the target. The amount of material ejected from each ion collision is dependent on the target material, yielding a highly material specific deposition rate. In the case of a deposition of

elemental metals, simple DC sputtering is usually used. During deposition of insulating materials an RF plasma must be used. By including reactive gasses e.g. oxygen in the plasma during the sputtering process, a thin film with atoms incorporated from the reactive gas can be achieved.

As shown in Figure 15, In the sputtering process, a plasma is created from
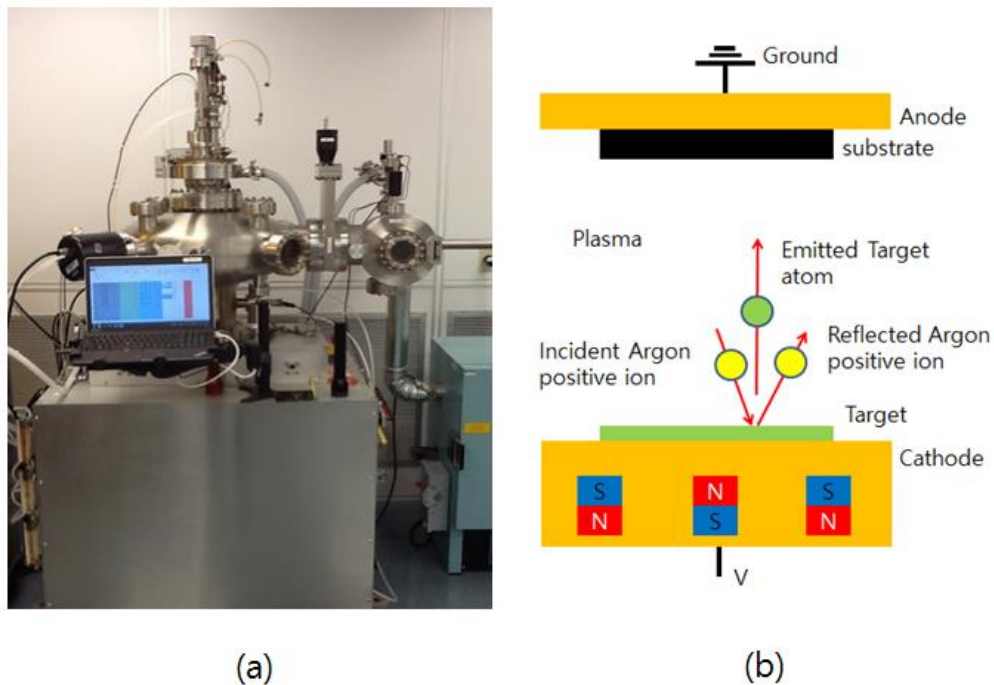
Figure 15   Magnetron sputtering system (a) Magnetron sputtering experiment Equipment_Kurt J. Lesker Corp   (b) Magnetron sputtering system schemetics

an inert gas like Ar, loaded into the vacuum chamber,by applying a high voltage between two electrodes on the magnetron. The plasma is concentrated right above the target material by magnets inside the magnetron. Atoms ejected from the target will deposit on all surfaces they strike and build up a thin film.

The deposition chamber is evacuated to pressures of 5x10^-6 Torr. The silver

Target, which is a Ag 99.99% pure, 2.00" diameter x 0.250"thick, made by Kurt

J. Lesker Corp was used in the study.   The only experimental technique is

coating the prism to the correct film thickness. The rate of deposition of metal is

different to each other. The thickness of the silver layer was 30-80nm to enable a

very sharp and deep guided wave resonance at the working wavelength which

was 632.8nm. Too thick a film will appear opaque while too thin a film will

appear semitransparent. When the surface plasmon resonance is not observed, the

thickness of metal needs to be checked to detemine whether it is correct. The

process of sputtering takes a few minutes depending on the desired thickness of

metal.

3.2   Experimental design

The light source used was a 25mW, CWoutput, 632.8nm He-Ne laser

(Melles Griot He-Ne Gas Lasers).   A Newport model 830 iris was used for the

small diameter of laser. A Newport mirror was used to adjust the light path

(model P100-P). A Newport linear polarizer controlled the polarization of He-Ne

Laser. A polarization rotator was used to switch between the TM mode and TE

mode of the laser. A high resolution linear actuator(PI:Physik Instrumente,

Modell: M-030DS) was used for high resolution of angle increment. A precision

rotation stage was used to increment the angle of the prism. System's linearity was proved as shown in Figure 17,. A high resolution linear actuator and rotation stage exhibits a high linearity to each other. And The system is accurate to ± 0.18 degrees at each measurement time. Because, the typical plasmon angular gap is very small. It depends on metal and dielectric material's type and character. In this case, when a silver film of and dielectric surface of air is used for plasmon, the gap of the angle is about 0.8 degrees. This case is for a highly conductive metal like silver and gold. When a metal with a high real dielectric component and large imaginary dielectric component was used for the plasmon, the gap of angle is typically above 10 degrees. In this case, the dip is quite shallow. Instead of dip in reflectivity, a peak of reflectivity was observed in reflectivity graph.

An optical power meter with a visible range detected the He-Ne laser. A Vernier Labpro was used for delivering data from power meter to the computer. The data were analyzed by Microsoft Excel. The equipment setup in the lab and schematic of the experimental setup are shown in Figure 16.
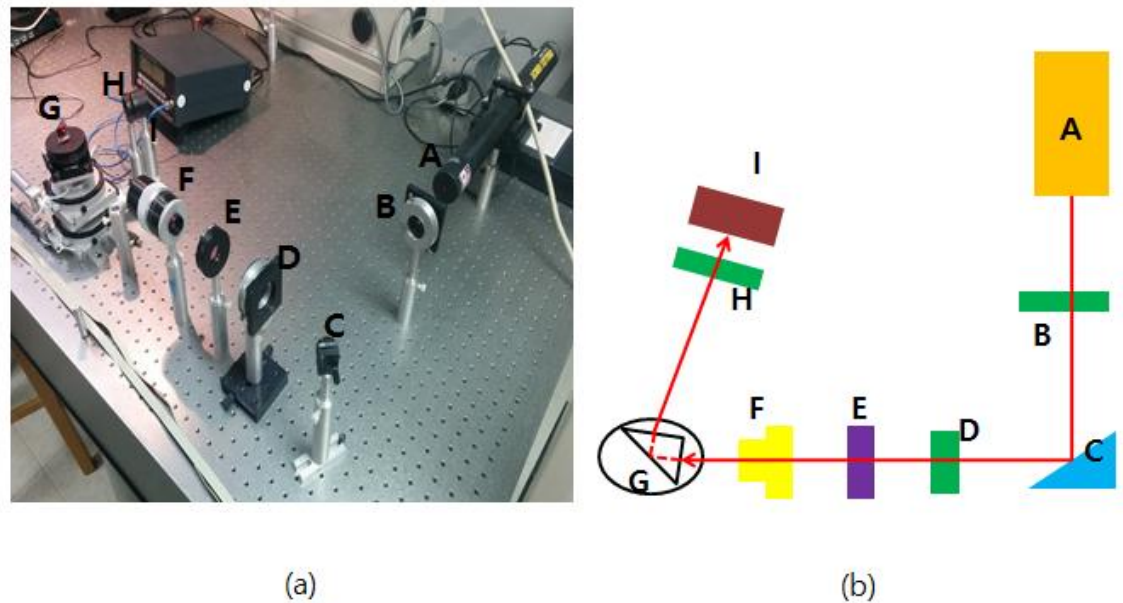
Figure 16 Experimental setup (a) Experimental setup in Lab (b) schematic of experimental setup detail schematic of the experimental setup A: Laser-diode B: IRIS   C: Mirror   D: IRIS   E: Linear polarizer   F: Polarization rotator G: Coated prism on a rotation stage with linear actuator   H: IRIS   I: Power meter

In this study, we used the TM mode polarization which is an orthogonal to the TE mode. With the TM mode laser polarization, we can check the Brewster angle of blank prism which is indicated by a reflectivity minimum before the angle of TIR. As described previous chapter, a surface plasmon polariton doesn't occur with TE mode polarization. As shown in Figure 16, the linear polarization, which is 'E' and polarization rotator, which is 'F', was used for TM mode polarization.

The prism with the thin film metal surface was mounted on a rotation stage, which was connected to linear actuator. When the measurement starts, the power meter rotates along with the reflected light. As shown in Figure 16, the rotation stage is also connected to the power meter which is 'I'. The bottom stage is connected to the power meter for rotating power meter, and the top stage is for changing the angle of incident into the prism. The bottom stage is rotated at twice the rate of the top stage. This is cause, in this system, the laser doesn't move at all to change the input angle. As shown in Figure 16, when the top stage moved to change the incident angle of prism, the angle is changed between the laser and prism. However, It just happened at only those two. When the top stage, which is prism rotated, power meter has a negative angle with respect to prism. To compensate for system's behavior, the bottom stage, which represents the power meter should move twice as much as the top stage, which represents the prism.

These algorithms were input into the software, which controls the prism and power meter angle. The LabPro analyzer takes signal of light intensity from the power meter while the program runs. The data are taken from the LabPro analyzer and moved to Excel file. These data are shown in Chapter 4.
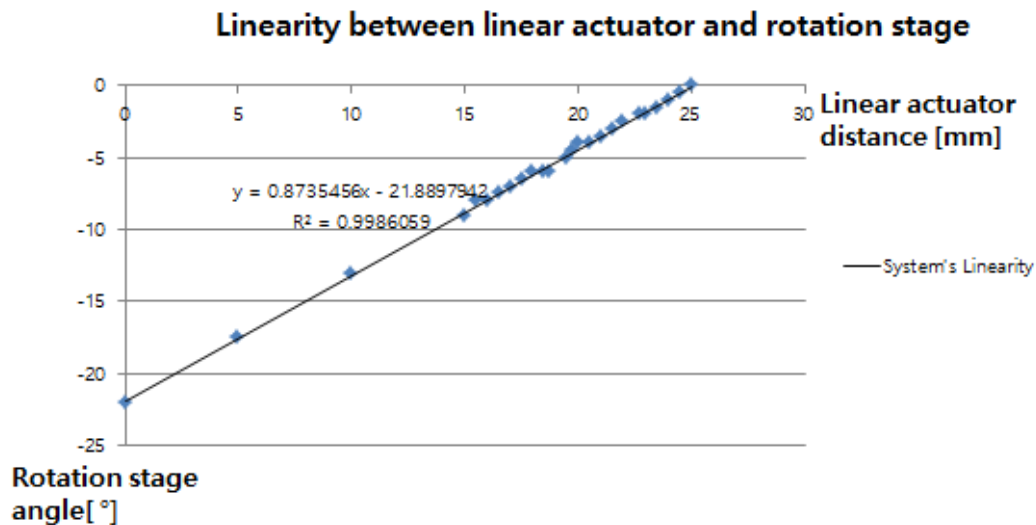
Figure 17   Rotational stage of linearity

Table 1   Linearity data

Linear motor distance[mm]	Angle [degree]	Linear motor distance[mm]	Angle [degree]	Linear motor distance[mm]	Angle [degree]
25	0	20.5	-4	16.5	-7.5
24.5	-0.5	20	-4	16	-8
24	-1	19.75	-4.5	15.5	-8
23.5	-1.5	19.5	-5	15	-9
23	-2	18.75	-6	10	-13
22.75	-2	18.5	-6	5	-17.5
22	-2.5	18	-6	0	-22
21.5	-3	17.5	-6.5		
21	-3.5	17	-7		

3.3 Profiler data for thickness of Ag

The glass slide which is soda-lime glass with the standard ISO 8037/1 was used to creat a control specimen for checking the thickness of the silver layer. This glass slide has surface 75mm x 25mm and 1mm thick (Cat. No. 16004-422). After sputtering the desired thickness of silver onto the glass slide, the Stylus Profiler was used for measuring the thickness of silver. The D-500 Stylus Profiler has the nanometer resolution to measure height. And also includes advanced optics and enhanced video controls for highly versatile sample visualization, as shown in Figure 18.
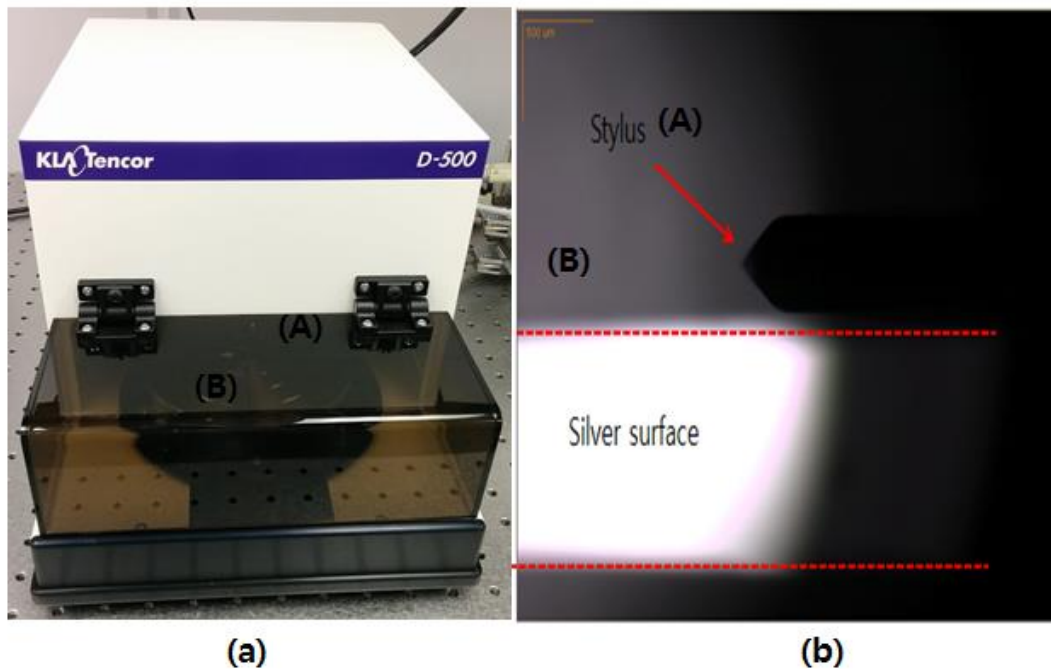
Figure 18   Profiler system (a) D-500 Stylus Profiler A: Stylus B: Sample plate   (b) Stylus Profiler visual image A: Stylus B: Sample plate

To measure the thickness of the layer correctly, the calibration was performed before measurement. The Stylus speed was 0.07mm/s and the stylus force was 15.0mg. As shown in Figure 19, the silver layer was deposited on both thickness the hypotenuse of prism and the glass slide at the same time. We performed measurements using thecontrol sample, and characterized its surface. Each thickness exhibits a different dielectric function.
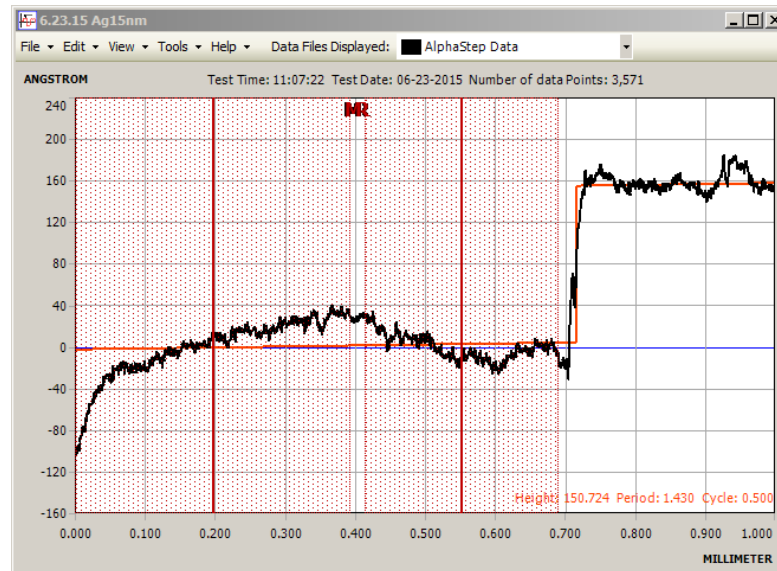
Figure 19 Ag 17nm thickness of AlphaStep Data

As shown in Figure 20, the second measurement of Ag thickness is 35nm. the red mesh is considered to be the original surface, which is flat. The value of the measurement is the difference between the red mesh area and the other area.
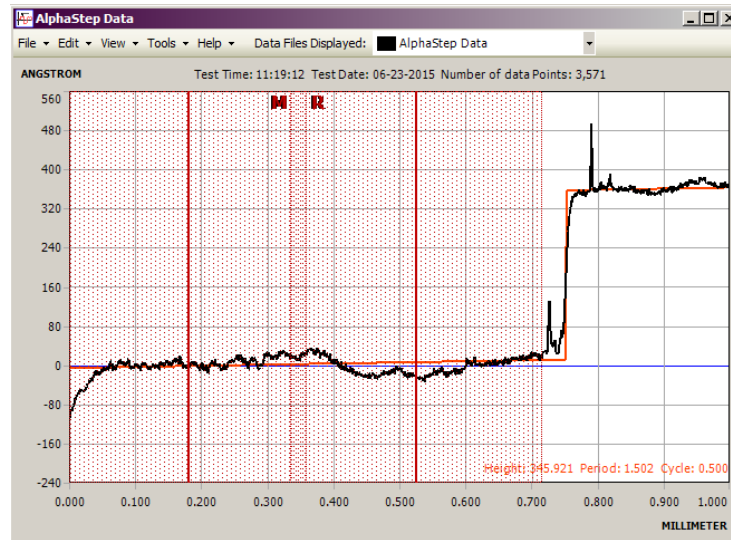
Figure 20   Ag 35nm thickness of AlphaStep Data

As shown in Figure 21,   the third measurement of Ag thickness is 57nm. The error of thickness is small in the third sample even though the thickness of metal is much bigger than the other one.

Figure 21 Ag 57nm thickness of AlphaStep data

Table 2   Thickness raw data

	#1	#2	#3
1	16.5nm	36.1nm	57.5nm
2	17.2nm	35.8nm	58.2nm
3	16.9nm	35.2nm	57.1nm
4	17.1nm	35.6nm	56.2nm
5	17.3nm	37.1nm	56.1nm
Standard deviation(STD)	0.282843	1.232071	0.944458
Average value	17nm	35.96nm	57.02nm

Each time the thickness of the layer was measured five times each and the average value was report. When the deviation between values is above, the calibration of the profile was performed to get the correct value.

3.4 Spectroscopic Ellipsometry

The ellipsometer was used for determining the complex dielectric constant of the silver film. ellipsometry is a non- destructive optical technique in which the sample is characterized to be illuminated with a beam of polarized light. As shown in Figure 22, the ellipsometer basically consists of laser, analyzer and photo detector.
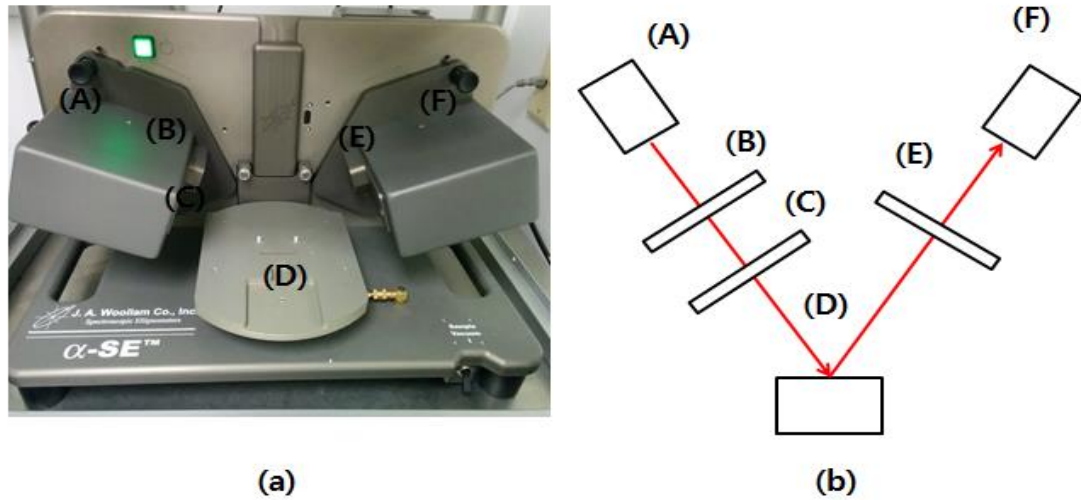
Figure 22   Ellipsometer system (a) Lab equipment (b) Ellipsometer schematic : (A) Light Source(Laser) (B) Polarizer (C) Wave Plate (D) sample   (E)Analyzer (F) Photodetector

Ellipsometry measures the change in polarization state of the measurement beam induced by reflection from the sample. Typically, the ellipsometric Psi(Ψ) and Delta(Δ) parameters were used for characterizing the change in polarization state[21]. The change equation is

$$\tan(\Psi) * e^{i\Delta} = \rho = \frac{r_p}{r_s}$$

Here, ρ is the ratio of the reflectivity for p-polarized light r_p, which is the TM mode divided by the reflectivity for s-polarized light r_s, which is TE mode. The parameter ρ is a complex number and the ellipsometric parameters simply report these values in polar form. The value $\tan(\Psi)$ is the magnitude of the reflectivity ratio term, while Δ is the phase term.

In spectroscopic ellipsometry(SE), Ψ and Δ are acquired as a function of wavelength. This information in the data determines the sample characters. The film thickness, optical model, which is what substrate and metal is used need to fit the data set. The CompleteEASE software provides a graphical user interface for building models and displaying measured data. The Ellipsometer data which were converted to the complex dielectric function were used for Simon's simulation.

As shown in Figure 23, The Ψ and Δ values were transferred to the metal's dielectric function, which is -18.42 real number and 0.375 imaginary number for the 632.8nm wavelength. That means this material layer absorbs the very small amount of the light. The real number is a key factor in determining the plasmonic resonance angle.
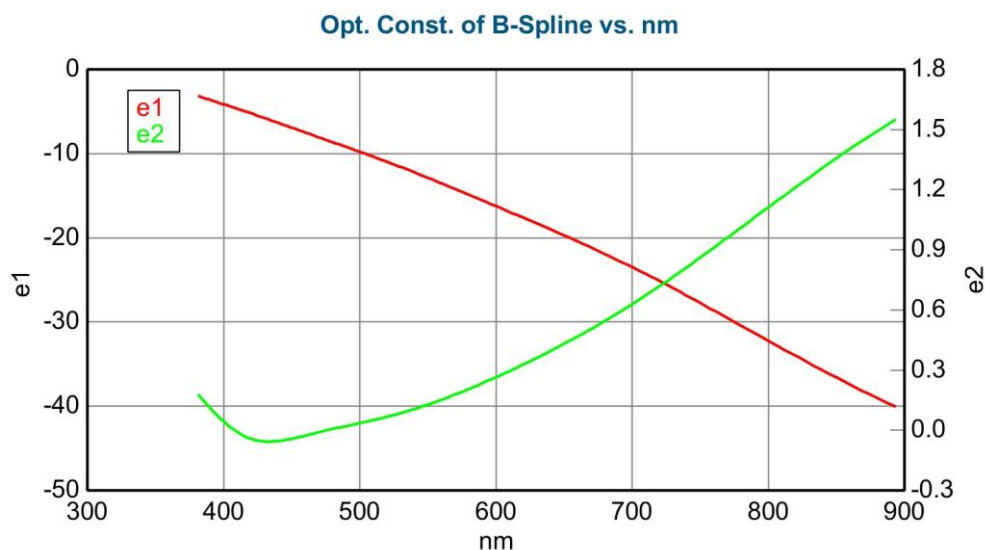
Figure 23 Ag 17nm film with glass substrate of the ellipsometer measurement data

As shown in Figure 24, The Ψ and Δ values was transferred to metal's dielectric function, which has -18.7 real number and negative value imaginary number at 632.8nm wavelength. The real number of metal film has similar value with Ag 17nm film, because the dielectric function of the metal layer is dependable more the type of metal than on the thickness of metal.[22,23]
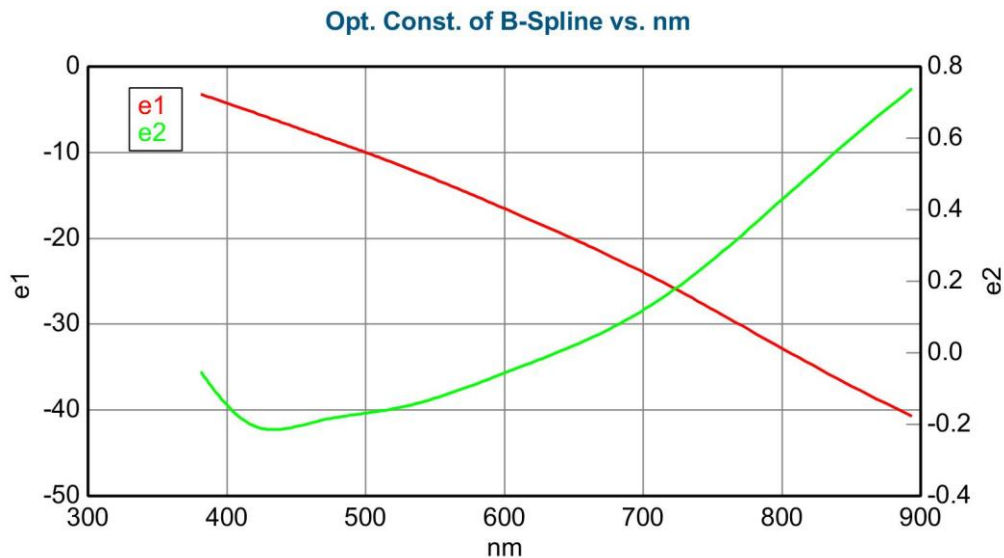
Figure 24 Ag 35nm film with glass substrate of the ellipsometer measurement data

As shown in Figure 25, The Ψ and Δ values was transferred to metal's dielectric function, which has -18.3 real number and 0.4 imaginary numbers in the 632.8nm wavelength. As shown in previous Figure, the three different thickness of ellipsometer data are very similar to each other. This will be discussed in the next chapter.
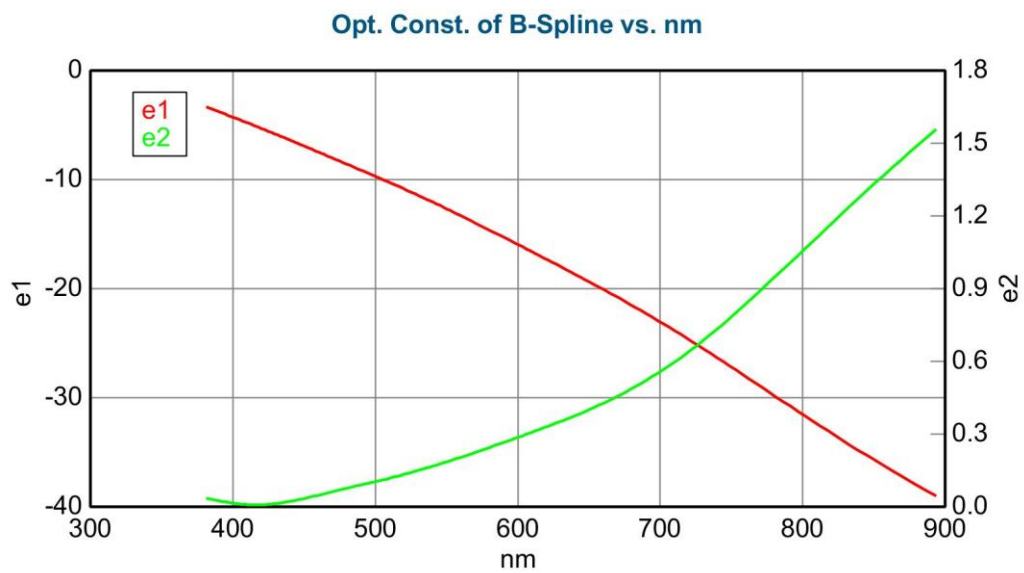
Figure 25 Ag 57nm film with glass substrate of the ellipsometer measurement data

4. Experimnets result and Analysis

We discussed Maxwell model for surface plasmon resonance, which shows us that why the plasmon effect exists and how it is related to surface dielectric function. Metamaterials were introduced using the Lorentz model. Metamaterials are artificial metallic structures having simultaneously negative permittivity and negative permeability otherwise known as double negative medium(DNG). This DNG medium has several features that any natural medium doesn't have such as negative refraction, evanescent wave amplification and backward phase. As a result of these, metamaterials don't obey Snell's law and Doppler effec. Due to this unique character of metamaterials, the concept of making a perfect lens with metamaterials has attracted attention in these days.[24,25]

In this chapter, we are going to discuss the fact that an Ag thin film can be a convenient candidate for metamaterial over specific range of frequencies. This is because, the thin film metal has a disk shape island structure itself. This structure is considered as the metamaterial unit. To model the metamaterial for each thickness of silver, we use surface plasmon-polaritons which are called SPPs. It can coupled Prism and metal to check where is plasmon resonance angle and how reflectivity of system is shown. This specific angle is function of metal and dielectric of thickness and metal's real and imaginary number of permittivity and dielectric layer's real and imaginary number. Each different thickness of Ag

has its own reflectivity depending on the angle of the system. After that, we are

going to find out which metamaterial model is well fitted and how much fit each

other at 632.8nm wavelength.

4.1 Experiments result & Maxwell Model

As described in the previous chapter, we built the experiment setup for

surface plasmon polariton. The simulation of Simon described in the

experimental result is reasonable and reliable. The ellipsometer data and Stylus

Profiler data as shown in the previous chapter was adopted for the simulation of

Simon.

As shown in Figure 26, the experiment result and Simon's simulation fit

each other well. The surface plasmon resonance angle(θp) is 44.88 degrees. But as

shown in Figure 26, the valley of the resonance point is hard to see. We check that a layer

which is less than 30nm thick will produce a shallow valley of reflectivity. If the surface

plasmon resonance is not observed, the thickness of metal should be different. Typically,

the thickness of silver should be between 30 and 80nm to see the clear valley of

reflectivity as shown in Figure 27, Figure 28. To employ Simons simulation, we used a

37nm thick film, with dielectric constant -18.42 + 1.2i, coating a prism of refractive index

1.457 at 632.8nm incidence as described in Table 3.

`

Figure 26   Comparison between Ag17nm and Simon's Simulation

As shown in Figure 27, the experiment result and Simon's simulation fit each other well. The surface plasmon resonance angle(θp) is 44.89 degrees. As commented previously, the valley of the resonance point is very clear between 30nm and 80nm ranges. To do the simulation of Simon, we used the thickness of silver, which is a 35nm and the refractive index of Prism, which is 1.457 at 632.8nm and metal's dielectric function, which is -18.32+1.26i   as described in Table 3.
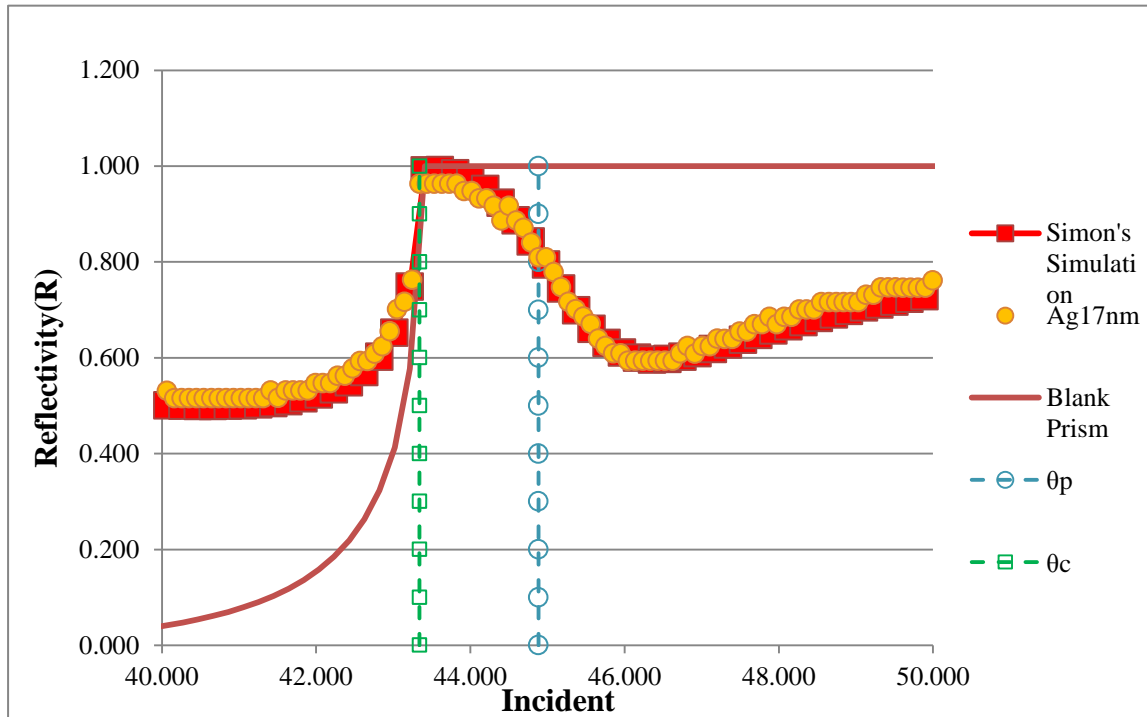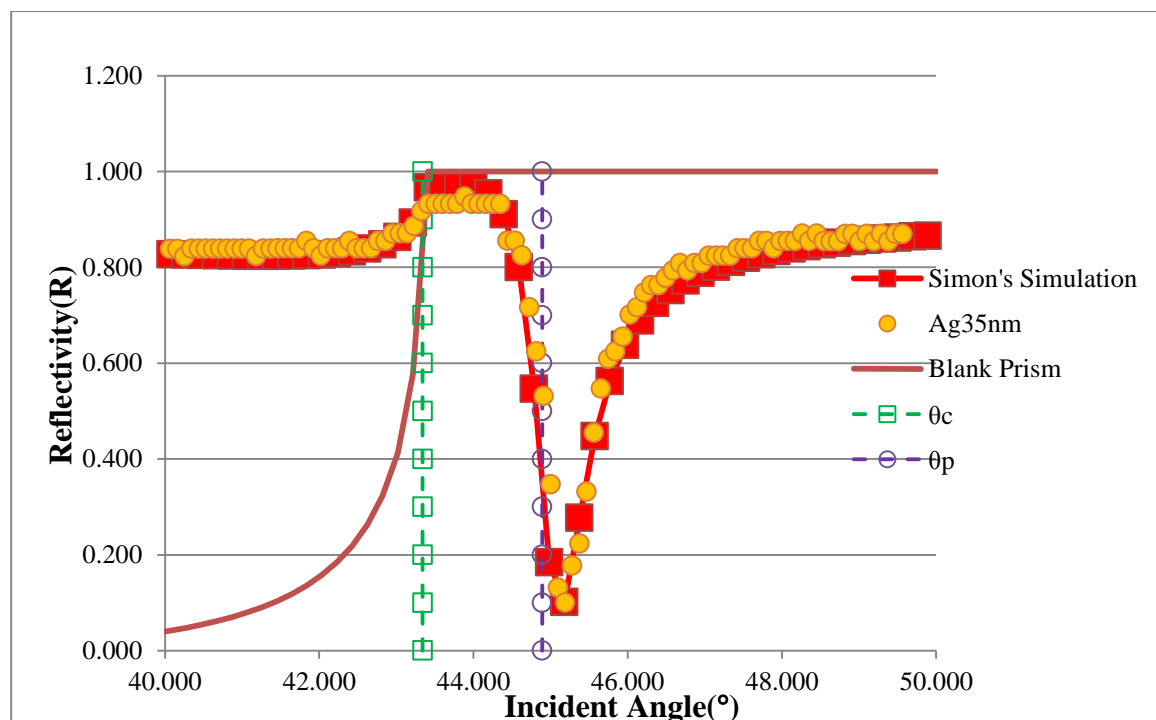
Figure 27   Comparison between Ag35nm and Simon's Simulation

As shown in Figure 28, the experiment result and Simon's simulation fit well each other. The surface plasmon resonance angle(θp) is 44.88 degrees. And the valley of plasmon resonance angle is quite sharp. One thing that we need to make sure of is that the surface plasmon resonance angle which is θp is not a function of the thickness of the metal. As shown in the previous figure, θp is almost constant even if the thickness difference is double or triple. But as you can see in Figure 26, Figure 27, Figure 28, the reflectivity depends on the angle is different for each plot. This is because the high mass thicknesses cause the nano-islands to form larger sizes. If the mass thickness is large enough, the metal layer becomes eventually almost completely continuous. To do the simulation of Simon, we used the thickness of silver, which is a 35nm and refractive

index of Prism, which is 1.457 @ 632.8nm and metal's dielectric function, which is -

18.42+1.2i　as described in Table 3.
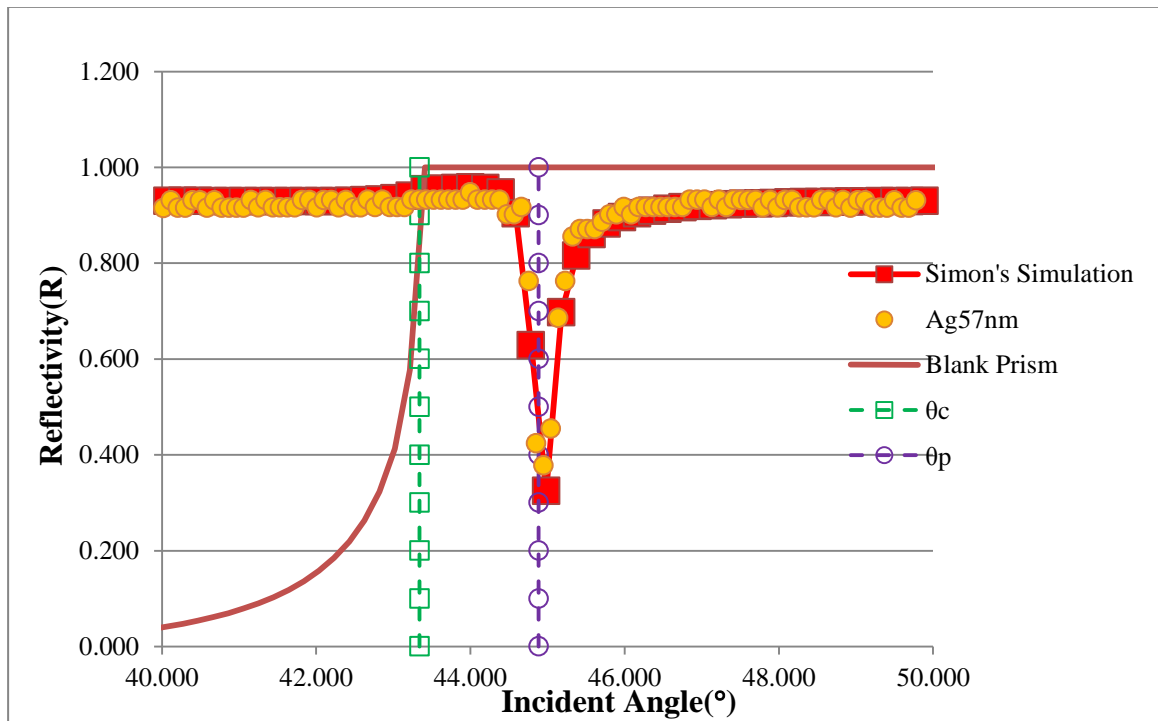
Figure 28　　Comparison between Ag57nm and Simon's Simulation

Table 3   Simon's simulation data table

Specimen	Ag17nm	Ag35nm	Ag57nm
n prism	1.457	1.457	1.457
t (Å)	170	350	570
λ (Å)	6328	6328	6328
ε (real)	-18.42	-18.32	-18.42
ε (imaginary)	1.2	1.26	1.2
Ɛp	-18.42+1.2i	-18.32+1.26i	-18.42+1.2i
θp (degrees)	44.88	44.89	44.88
θc (degrees)	43.34	43.34	43.34

4.2   Annealing Ag film

We deposit silver island films by evaporating silver on the prism hypotenuse surface at very low evaporation rates about 4.6 A/s in vacuum environments. The silver thicknesses used were is 17nm, 35nm and 57nm.

To change plasmon resonance peak, the silver layer was annealed at 150℃ for a 10 minutes in the oven. The annealing process usually makes the size of diameter of silver structure bigger than it was. When Ag was annealed at 150℃, the Ag layer is partitioned into an outer layer of Ag_2O_3 on a substrate of Ag.

The annealing process typically makes the structure of thin layer surface bigger than it was. As shown in Figure 29, when the thin film of metal surface

was adopted by annealing, the silver oxide dielectric function is also changed as

shown in Table 4, Figure 29.

Table 4 Annealing Data

Case	Ag thickness	Annealing Temperature	Annealing Time
#1 sample	35nm	0	0
#2 sample	35nm	150	10 min
#3 sample	35nm	200	10 min
#4 sample	35nm	400	10 min
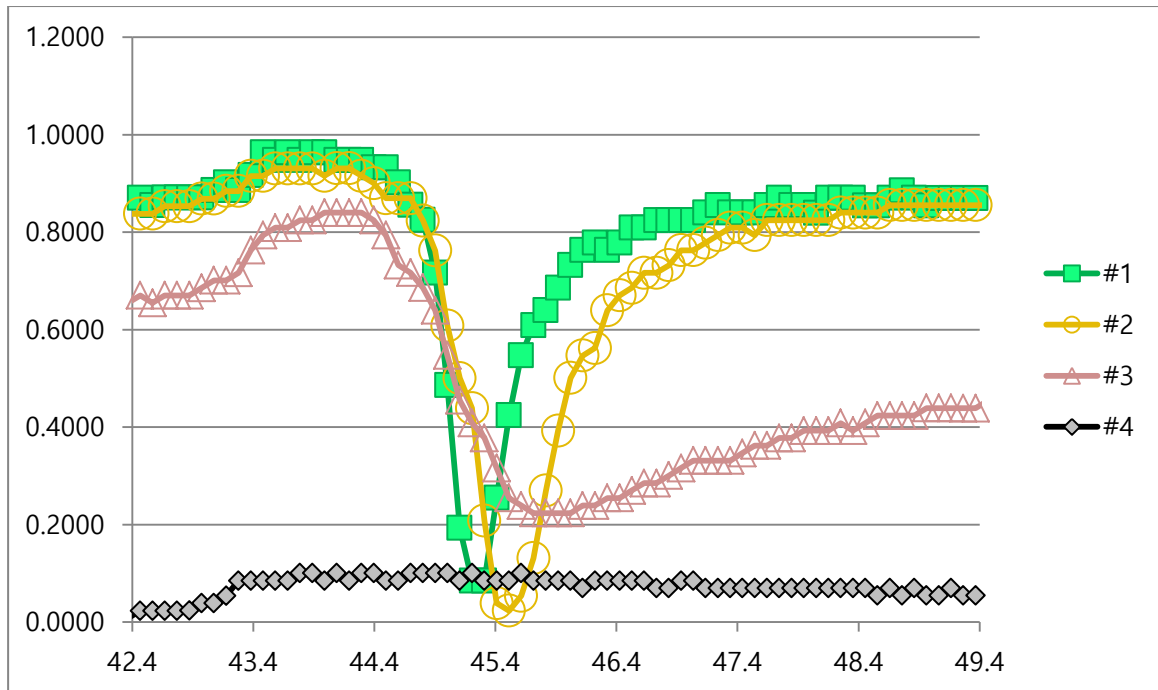
Figure 29 Silver layer annealing to change SPR angle

4.3   Equivalent Metamaterial Model for the experiments result

As previously mentioned, the thin film metal has nano-islands,which are about 30nm-200nm diameter. It depends on deposition rate of sputtering machine and mass Thickness. It also varies with annealing method. To find an equivalent matermaterial model of thin the silver layer, we choose COMSOL software. This COMSOL model basically imitates the nano-islands which can be shown in thin film metal. The surface plasmon resonance exists in thin film metal. As shown in Figure 14, the top part consists of silica glass, which has a refractive index of 1.457 at 632.8nm. The bottom part consists of air, which has a refractive index of

1.002765 at 632.8nm. The middle part is a dielectric material, which has relative permittivity, relative permeability and zero electric conductivity. As previously mentioned, there are two assumptions in the COMSOL model. First, when the thickness of metal is small enough with respect to incident wavelength,which is about 630nm, the thickness of metal is modeled as a perfect electric conductor(PEC). Second, we have discussed surfaces in terms of their reflective coefficient. Using duality, we can produce surfaces having an analogous transmission coefficient. This duality principle is often referred to as the Babinet's principle. To see the similarity of this COMSOL model for the each silver layer, we have discussed the reflective coefficient. In this study, the COMSOL model is basically used as a complementary model with a thin silver layer. The thin silver layer has a nano-island metal part of its surface. However, the equivalent COMSOL model has holes instead of metal parts as shown in Figure 14. As mention previously, using duality, we can produce surfaces having an analogous transmission coefficient. That should be exactly opposite between transmission coefficient and reflective coefficient.[26,27]
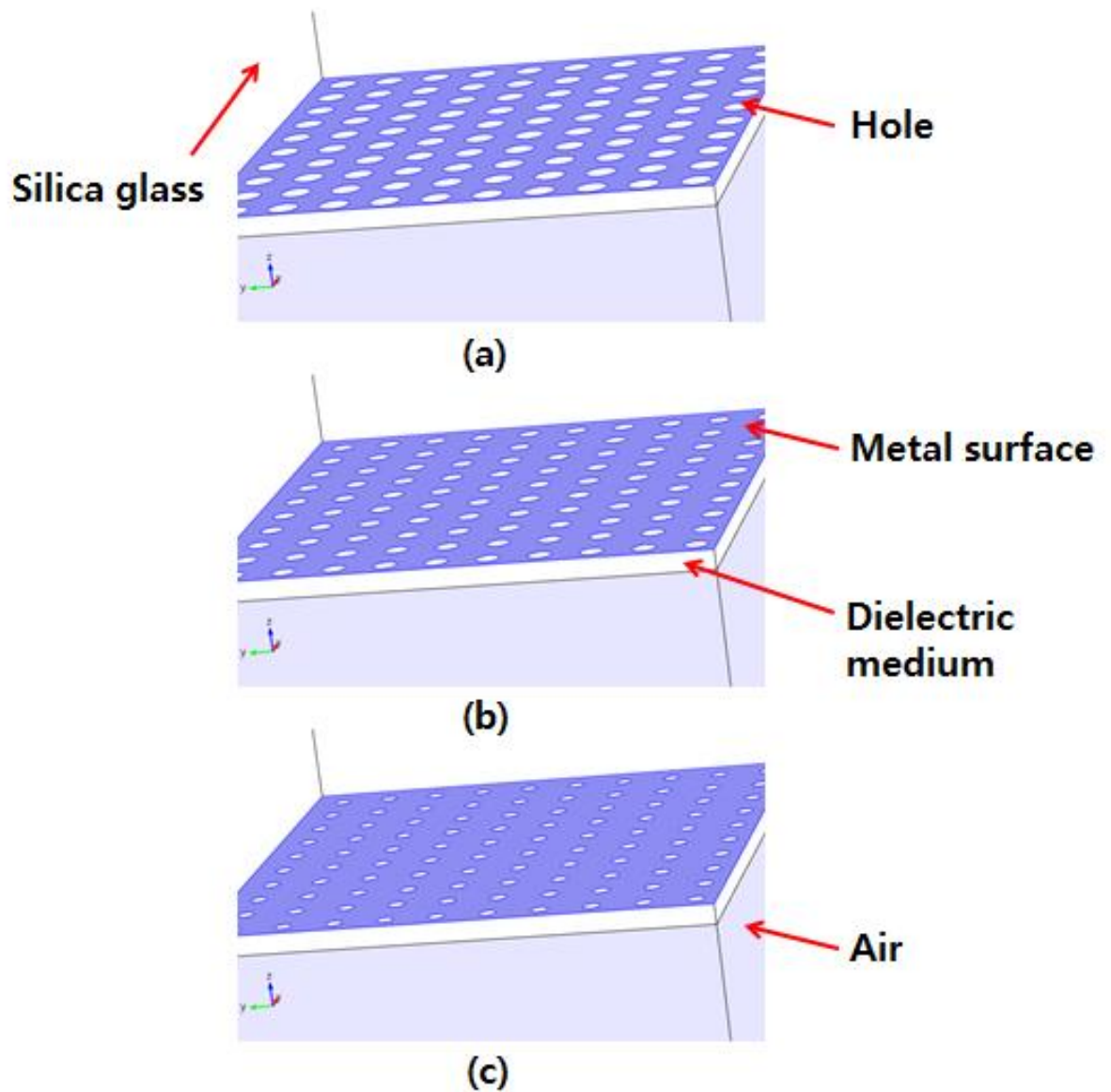
Figure 30   COMSOL Model   (a) Model #1(Silica glass / Relative Permittivity of dielectric real number 2.17 / Air) with respect to Ag17nm   (b) Model #2 (Silica glass / Relative Permittivity of dielectric real number 1.97 / Air) with respect to Ag35nm (c) Model #3 (Silica glass / Relative Permittivity of dielectric real number 2.95/ Air) with respect to Ag57nm

As shown in Figure 31, equivalent metamaterial model #1 is similar to the

Simons' simulation. This model is the worst fit model among the others.

Table 5 COMSOL Equivalent Model character with respect to each thickness of silver

	Model #1	Model #2	Model #3
Target silver thickness(nm)	17nm	35nm	57nm
COMSOL Equivalent disk radius	147nm	110nm	80nm
Period	500nm	500nm	500nm
Substrate Relative permittivity	2.17	1.97	2.95
Substrate Relative permeability	1	1	1
Substrate Thickness	200nm	200nm	200nm
Top part material	Silica glass	Silica glass	Silica glass
Botton part material	Air	Air	Air

As shown in Table 5, The Ag17nm of   equivalent model has a 147nm

disk hole which is quite a small metal part among the others. It makes sense that

when the thickness of the mass is small, the metal part is also small on the

surface which means nano-island is par away each other. And to do imitate the

experimental system, the Equivalent model has Silica glass material in the top

part and Air in the bottom part.

Figure 31   Reflectivity vs Incident angle of Prism with Ag 17nm + Equivalent COMSOL MODEL #1

As shown in Figure 32, the experimental result of Ag 35nm is fitted well

with the equivalent COMSOL model #2. The model has a 110nm radius hole

disk, which is a much smaller hole, between metal parts. That means when the

metal is thick the nano-island is larger and the islands are closely arranged.

That's why the overall reflectivity of Figure 32 is also much higher than Figure 31.

The equivalent model of the substrate is also very important role to match with

surface plasmon resonance angle. When the relative permittivity of substrate is changed by 0.1, the plasmon resonance angle is also moved by about 0.3 degrees. It is basically linear when it is in a specific range.
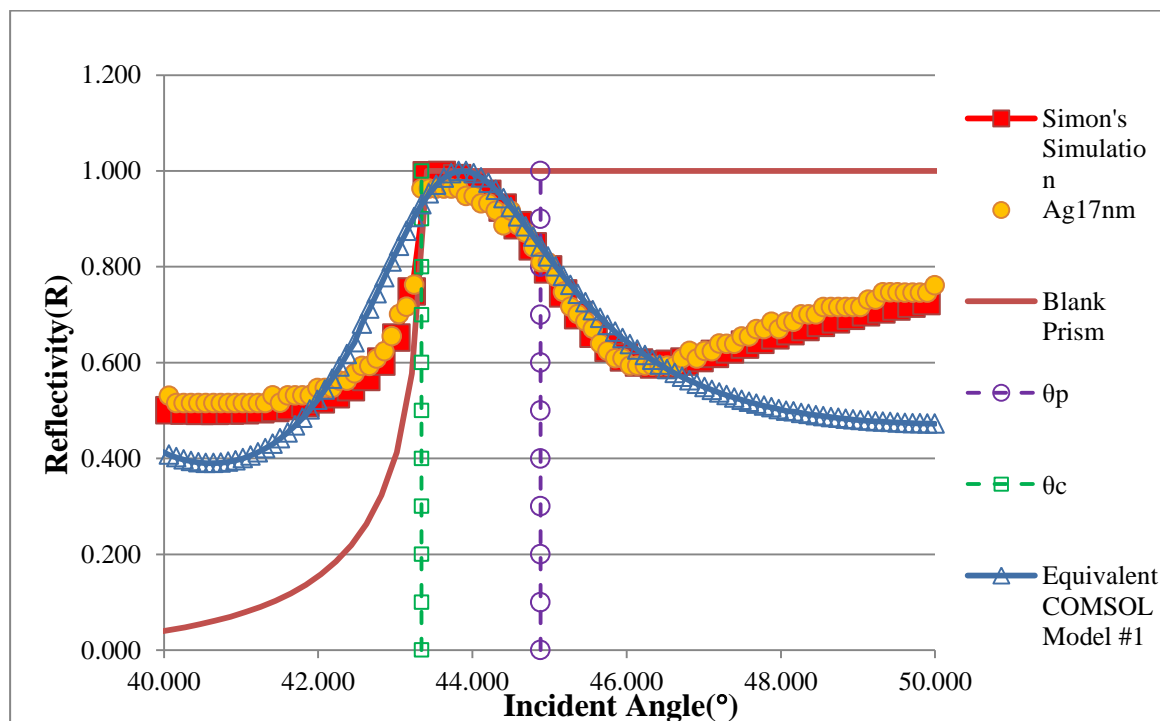

Figure 32   Reflectivity vs Incident angle of Prism with Ag 35nm + Equivalent COMSOL MODEL #2

As shown in Figure 33, the experimental result of Ag 57nm is fitted well with the equivalent COMSOL model #3. The model has an 80nm radius hole disk, which is a much smaller hole, between the metal parts than for the other models. That means when the metal is thick the nano-island is larger and the islands are closer to each other. And this equivalent model is the most well fitted in among the three equivalent models.
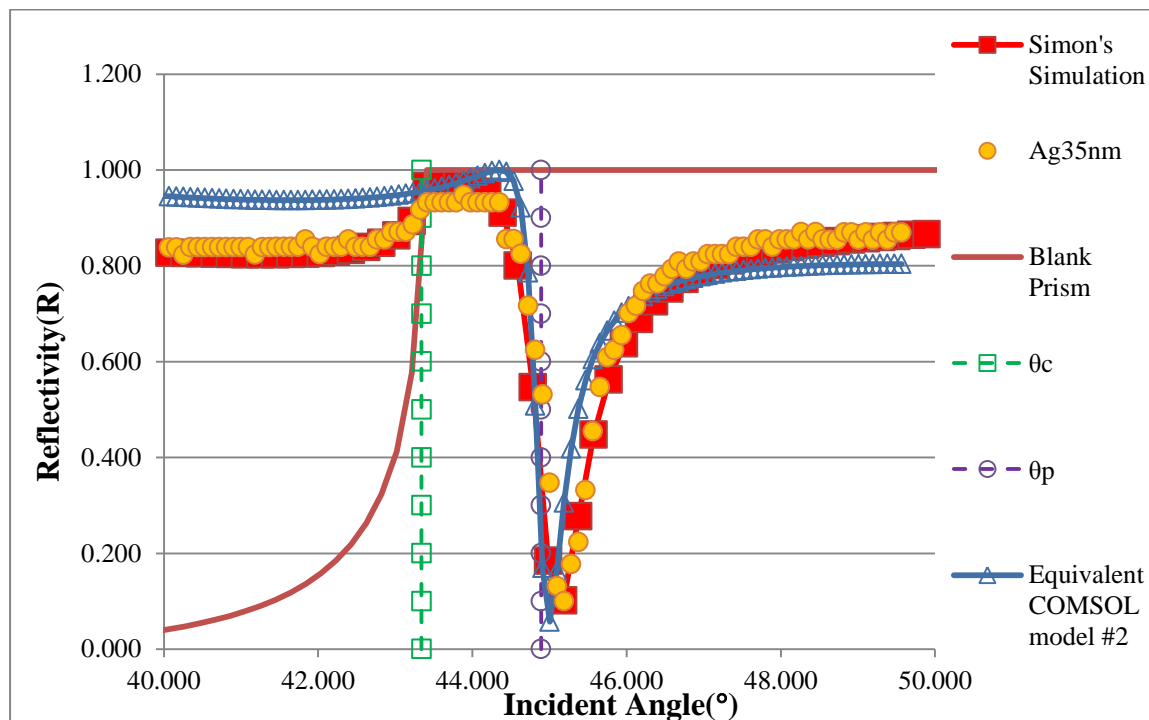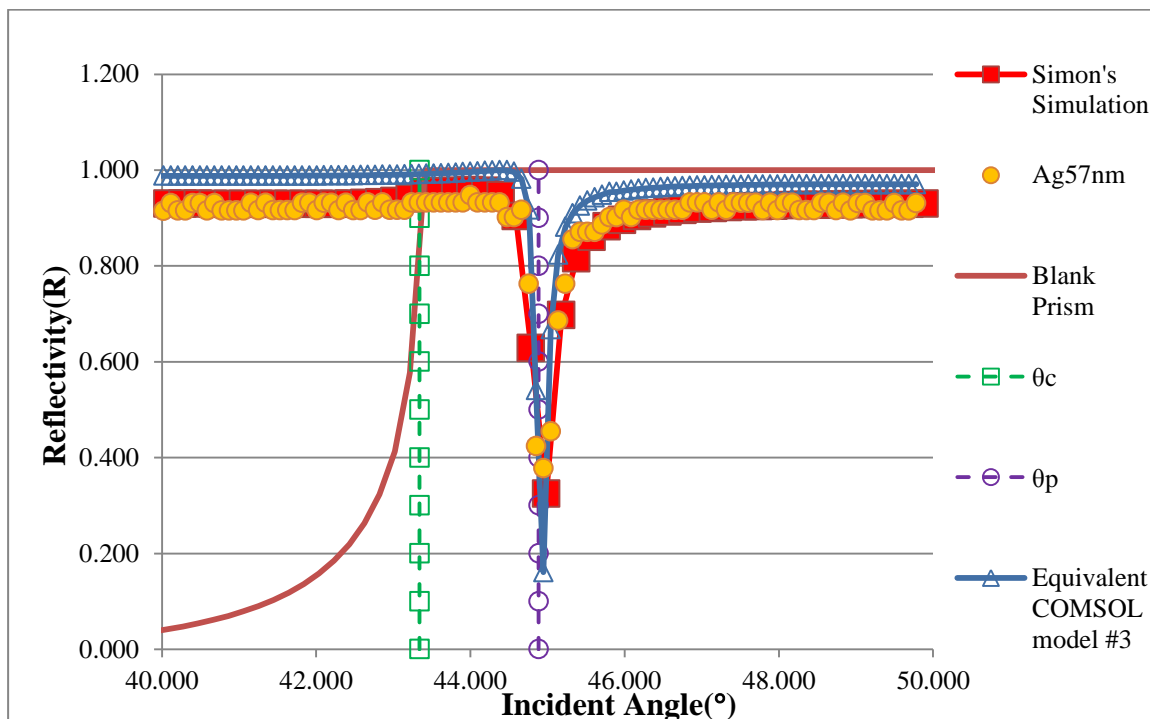
Figure 33   Reflectivity vs Incident angle of Prism with Ag 57nm + Equivalent COMSOL MODEL #3

As shown in Figure 34, the equivalent model #1 has a bandpass resonance near 475THz which is about 632nm wavelength. The s-parameter is commonly used to check Metamaterial frequency range.[28,29,30] As previously mentioned, metamaterial is a double negative medium over a specific frequency range. The bandpass resonance of the s-parameter plot is evidence that the specific circuit is a double negative medium at certain frequencies. In this Model, each disk has self inductance, and the disks have capacitance with each other. Those effective

inductances and effective capacitances can be a closed circuit like other

metamaterials.
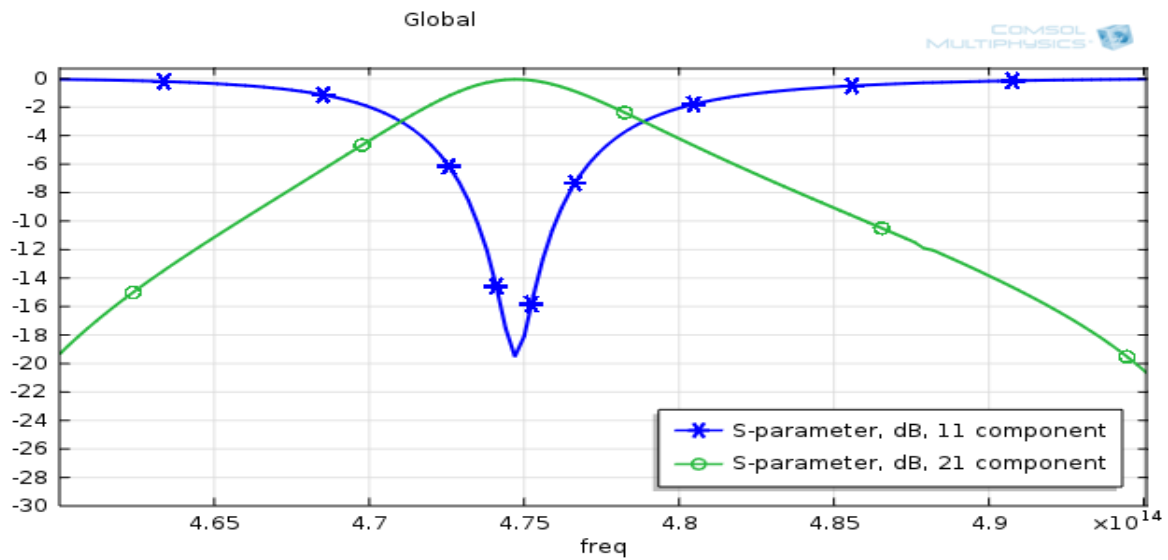
Figure 34 The S-parameter plot show a bandpass resonance near 475THz-Equivalent COMSOM MODEL #1

As shown in Figure 35, the equivalent model #2 has a bandpass resonance

near 444THz which is 675nm wavelength. At this frequency, the model has -

20dB less which means almost 99 percent of light is transmitted.
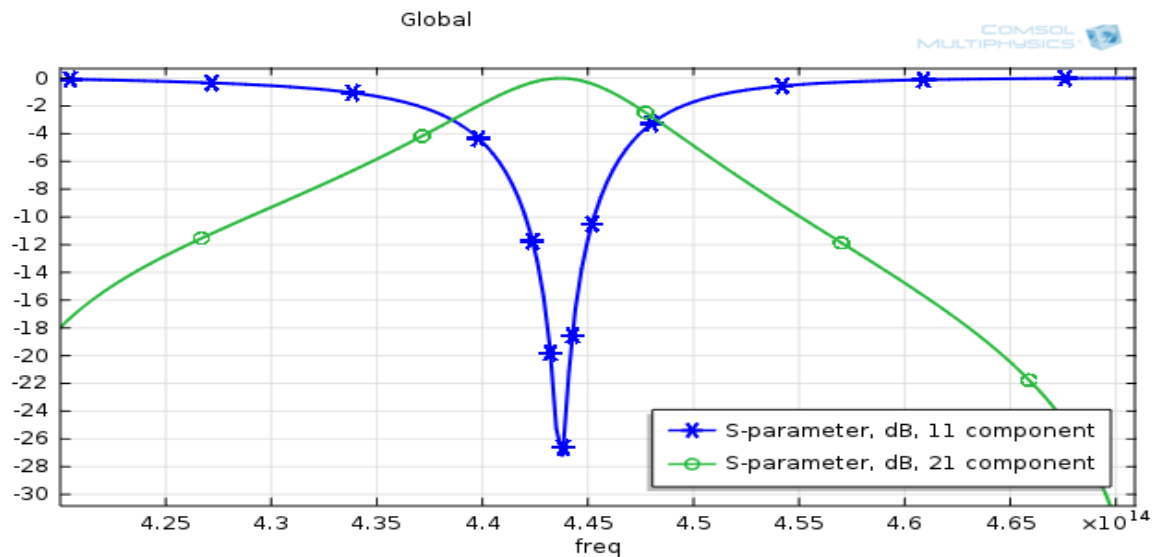
Figure 35 The S-parameter plot show a bandpass resonance near 448THz-Equivalent COMSOM MODEL #2

As shown in Figure 36, the equivalent model #3 has a bandpass resonance near 461THz which is 650nm wavelength. Each model has its own frequency range and value for metamaterial. This is because, each model has its own effective Inductance and effective capacitance. The different disk radii have a tremendous effect on its circuit value.
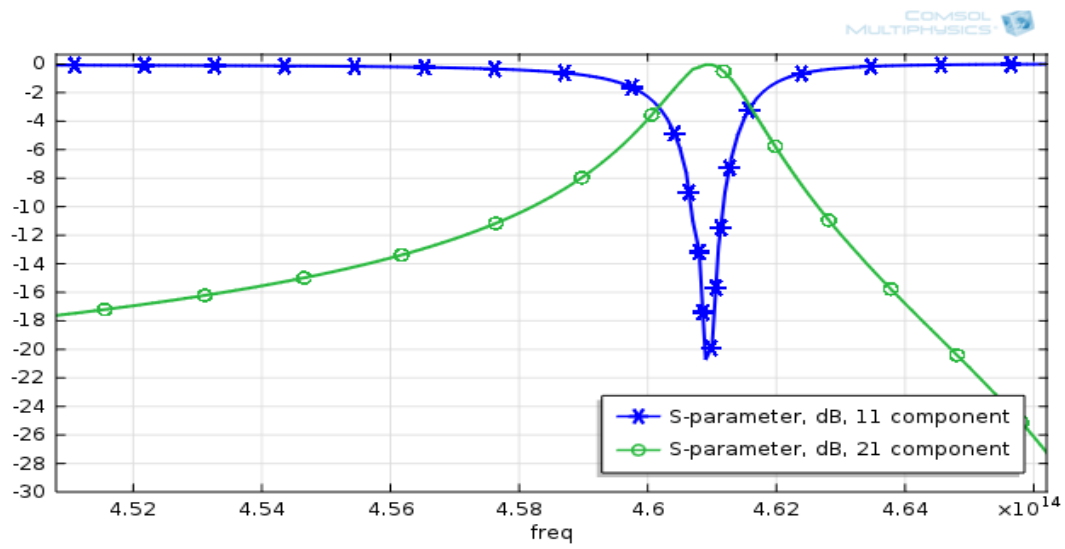
Figure 36   The S-parameter plot show a bandpass resonance near 461THz-Equivalent COMSOM MODEL #3

5. Conclusion and Future work

We observed that the 17nm, 35nm, 57nm thin silver layer's surface plasmon resonance angle doesn't change with respect to the thickness of metal. Even when the thickness of silver layer is changed about twice, the SPR angle remained about 44.88 ± 0.01 degrees. But the overall reflectivity is highly dependent on the thickness of the metal as shown in the previous figure. When the thickness of silver is less than 30nm and more than 80nm, the SPR is difficult to be observed. Even though the minimum of reflectivity couldn't be observed in the reflectivity graph, the Simon's simulation can exactly predict the reflectivity curves.

The movement of surface plasmon angle is observed about 0.5 degree, 1.2 degree when the 35nm of silver film metal was annealed at 150 Celsius, 200 Celsius for a 10 min in the oven, respectively. With this results, we can conclude when the metal was annealed, the thin film metal was transferred to silver oxide. That's why we observed deviation of plasmon angle. When the 35nm of silver film metal was annealed at 400 Celsius, the reflectivity is very low in a whole incident of angle. Because when the silver film was annealed at 400 Celsius, the most part of silver film metal turns into silver oxide layer.

As shown in the previous figure, we found an equivalent disk type of metamaterial model, which is modeled as a thin nano-island silver. The model #1 which acts as a metamaterial around 475THz, which is 631.6nm, has a disk of radius 147nm, and a substrate relative permittivity of 2.17. The model #2 which acts as a metamaterial around 444THz, which is 675.7nm,   has a disk of radius 110nm, substrate relative permittivity of 1.97. The model #3 which acts as a metamaterial around 461THz, which is 650.8nm, has a disk of radius 147nm, and a substrate relative permittivity 2.95. These nano-islands of metal can be obtained for thin film metal. That means thin film metal layers can be candidates for the metamaterial without fabricating each unit of the metamaterial. The disk radius can be changeable to metal's thickness, deposition rate, metal's character. The different disk size can be achieved by annealing thin film metal. It allows for the thin film metal layer to be satisfied with various frequency ranges.

We suggest a new fabrication method of metamaterials. We also showed a good agreement with the disk metamaterial model and thin silver layer's SPR. Further, we assumed that the thin silver layer is composed of nano-islands for nominally thin surfaces. To verify this, we should characterize the disk formation with various factors like thickness of metal, deposition rate, and type of metal. When the thickness of metal is modeled as a perfect electric conductor(PEC), it will be more accurate if the silver layer is much thicker than the skin depth in the simulated frequency range. However, the skin depth is smaller than the thickness of silver in the experiments. There is no way to build up with small thickness in

the COMSOL model because of limited computer memory. To make a more

accurate calculation, the mesh size of software should be smaller than it was.

LIST OF REFERENCES

[1] Wood, R.w. "XLII. On a Remarkable Case of Uneven Distribution of Light in a Diffraction Grating Spectrum." *Philosophical Magazine Series* 4,396-402 (1902)

[2] Otto, Andreas. "Excitation of Nonradiative Surface Plasma Waves in Silver by the Method of Frustrated Total Reflection." *Zeitschrift Physik Z. Physik* 216, 398-410(1968)

[3] Cooper, Matthew A. "Optical Biosensors in Drug Discovery." *Nature Reviews Drug Discovery Nat. Rev. Drug Disc.* 1,515-528 (2002)

[4] Karlsson, Robert. "SPR for Molecular Interaction Analysis: A Review of Emerging Application Areas." *J. Mol. Recognit. Journal of Molecular Recognition* 17,151-161 (2004)

[5] Boozer, Christina, Gibum Kim, Shuxin Cong, Hannwen Guan, and Timothy Londergan. "Looking towards Label-free Biomolecular Interaction Analysis in a High-throughput Format: A Review of New Surface Plasmon Resonance Technologies." *Current Opinion in Biotechnology* 17,400-405 (2006)

[6] R.S. Popovic, "Hall Devices for Magnetic Sensor Microsystems" (invited paper), Proceedings of the international conference on solid-state sensors and actuators Transducers'97, 101, 377-380 (1997)

[7] Gupta, B. D., and R. K. Verma. "Surface Plasmon Resonance-Based Fiber Optic Sensors: Principle, Probe Designs, and Some Applications." *Journal of Sensors* 2009,1-12 (2009)

[8] Pendry, J.b., A.j. Holden, D.j. Robbins, and W.j. Stewart. "Magnetism from Conductors and Enhanced Nonlinear Phenomena." *IEEE Transactions on Microwave Theory and Techniques IEEE Trans. Microwave Theory Techn.* 47, 2075-2108 (1999)

[9] Liu, Na, Hongcang Guo, Liwei Fu, Stefan Kaiser, Heinz Schweizer, and Harald Giessen. "Three-dimensional Photonic Metamaterials at Optical Frequencies." *Nature Materials Nat Mater* 7, 31-37 (2007)

[10] Lalj, Hicham, Hafid Griguer, and M'Hamed Drissi. "Very Compact Bandstop Filters Based on Miniaturized Complementary Metamaterial Resonators." *Wireless Engineering and Technology WET* 4, 101-104 (2013)

[11] Hosseini, M., and M. Hakkak. "Characteristics Estimation for Jerusalem Cross-Based Artificial Magnetic Conductors." *Antennas Wirel. Propag. Lett. IEEE Antennas and Wireless Propagation Letters* 7, 58-61 (2008)

[12] García-Meca, Carlos, Juan Hurtado, Javier Martí, Alejandro Martínez, Wayne Dickson, and Anatoly V. Zayats. "Low-Loss Multilayered Metamaterial Exhibiting a Negative Index of Refraction at Visible Wavelengths." *Phys. Rev. Lett. Physical Review Letters* 106,1-4 (2011)

[13] Dionne, Jennifer A., Ewold Verhagen, Albert Polman, and Harry A. Atwater. "Are Negative Index Materials Achievable with Surface Plasmon Waveguides? A case study of three plasmonic geometries" *Opt. Express Optics Express* 16, 19001-17 (2008)

[14] Chen, Tao, Suyan Li, and Hui Sun. "Metamaterials Application in Sensing."*Sensors* 12, 2742-2765. (2012)

[15] Prajapati, Y.k., Archana Yadav, A. Verma, V. Singh, and J.p. Saini. "Effect of Metamaterial Layer on Optical Surface Plasmon Resonance Sensor."*Optik - International Journal for Light and Electron Optics* 124, 3607-3610 (2013)

[16] Simon, H. J. "Surface Plasmons in Silver Films—a Novel Undergraduate Experiment." *Am. J. Phys. American Journal of Physics* 43,630-637 (1975)

[17] Veselago, V. G. "Electrodynamics of Media with Simultaneously Negative Electric Permittivity and Magnetic Permeability." *Advances in Electromagnetics of Complex Media and Metamaterials* 1,83-97 (2002)

[18] Marqués, Ricardo, Ferran Martín, and Mario Sorolla. *Metamaterials with Negative Parameters: Theory, Design, and Microwave Applications*. Hoboken, NJ: Wiley-Interscience (2008)

[19] Duyne, R. P. Van, J. C. Hulteen, and D. A. Treichel. "Atomic Force Microscopy and Surface-enhanced Raman Spectroscopy. I. Ag Island Films and Ag Film over Polymer Nanosphere Surfaces Supported on Glass." J. Chem. Phys. The Journal of Chemical Physics 99,2101-2115 (1993)

[20] Royer, P., J. P. Goudonnet, R. J. Warmack, and T. L. Ferrell. "Substrate Effects on Surface-plasmon Spectra in Metal-island Films." *Phys. Rev. B Physical Review B* 35, 3753-3759 (1987)

[21] H. Tompkins and E. Irene, eds. Handbook of Ellipsometry, William Andrew Publishing, 47-72 (2005)

[22] H. Fujiwara, Spectroscopic Ellipsometry Principles and Applications John Wiley & Sons, West Sussex, England (2007)

[23] J.N. Hilfiker and J.A. Woollam, *Ellipsometry*, in Encyclopedia of Modern Optics, edited by Robert D. Guenther, Duncan G. Steel and Leopold Bayvel, Elsevier, Oxford, (2004)

[24] Ekmekci, Evren, Kagan Topalli, Tayfun Akin, and Gonul Turhan-Sayan. "A Tunable Multi-band Metamaterial Design Using Micro-split SRR Structures." *Opt. Express Optics Express* 17,16046-58 (2009)

[25] Kafesaki, M., N. H. Shen, S. Tzortzakis, and C. M. Soukoulis. "Optically Switchable and Tunable Terahertz Metamaterials through Photoconductivity." *Journal of Optics J. Opt.* 14,114008-16 (2012)

[26] Bitzer, Andreas, Alex Ortner, Hannes Merbold, Thomas Feurer, and Markus Walther. "Terahertz Near-field Microscopy of Complementary Planar Metamaterials: Babinet's Principle." *Opt. Express Optics Express* 19, 2537-2545 (2011)

[27] Falcone, F., T. Lopetegi, M. A. G. Laso, J. D. Baena, J. Bonache, M. Beruete, R. Marqués, F. Martín, and M. Sorolla. "Babinet Principle Applied to the Design of Metasurfaces and Metamaterials." *Phys. Rev. Lett. Physical Review Letters* 93,197401-04 (2004)

[28] Rhbanou, Ahmed, Seddik Bri, and Mohamed Sabbane. "Design of X-band Substrate Integrated Waveguide Bandpass Filter with Dual High

Rejection." *Microwave and Optical Technology Letters Microw. Opt. Technol. Lett.* 57, 1744-1752. (2015)

[29] Garcia-Garcia, J., F. Martin, F. Falcone, J. Bonache, J.d. Baena, I. Gil, E. Amat, T. Lopetegi, M.a.g. Laso, J.a.m. Iturmendi, M. Sorolla, and R. Marques. "Microwave Filters with Improved Stopband Based on Sub-wavelength Resonators." *IEEE Transactions on Microwave Theory and Techniques IEEE Trans. Microwave Theory Techn.* 53, 1997-2006 (2005)

[30] Ekmekci, E., A. C. Strikwerda, K. Fan, G. Keiser, X. Zhang, G. Turhan-Sayan, and R. D. Averitt. "Frequency Tunable Terahertz Metamaterials Using Broadside Coupled Split-ring Resonators." *Phys. Rev. B Physical Review B* 83,193103-07 (2011)

APPENDIX

APPENDIX. A

Maxwell Simulation calculation.

This program calculates reflectance according to the model developed in Simon's Paper. It incorporates a thin film metal (e1+ ie2) sandwiched between a dielectric of index n and air.

> *restart*

> *with*(*plots*) :

> *assume*(*R*, '*real*');

> *assume*(*r12*,'*complex*', *r23*,'*complex*', *k*,'*complex*', *T2*,'*complex*', *R1*,'*complex*');

Insert the appropriate wavelength(wl) in angstoms, film thickness(d) in angstroms, index of refraction(n), complex dielectric function(ep) below.

> *wl* := 6328.0;

wl := 6328.0

> *d* := 350

d := 350

> $n := 1.457$

$n := 1.457$

> $ep := -18.4 + 0.4 \cdot I$

$ep := -18.4 + 0.4\ I$

θ1 refers to the angle incident to the prism.

θ2 refers to the refracted angle inside of the prism.

θ3 refers to the angle incident upon the thin film.

> $\theta1 := \arcsin(n \cdot \sin(\theta2))$

$\theta1 := \arcsin(1.457\ \sin(\theta2))$

> $\theta2 := \theta3 - \dfrac{Pi}{4}$

$\theta2 := \theta3 - \dfrac{1}{4}\ \pi$

k is the absorption coefficient for the E field in the metal.

> $k := -\left(\dfrac{I \cdot 2 \cdot \pi}{wl}\right) \cdot \left(ep - n^2 \cdot (\sin(\theta3))^2\right)^{0.5}$:

T2 is the cosine of the angle inside the thin film.

T3 is the cosine of the angle in the air ouside the thin film.

> $T2 := \left(1 - \dfrac{n^2 \cdot (\sin(\theta3))^2}{ep}\right)^{0.5}$:

> $T3 := \left(1 - n^2 \cdot (\sin(\theta 3))^2\right)^{0.5}$:

r12 is reflectivity at the silica - metal interface.

r23 is reflectivity at the metal - air interface.

> $r12 := \dfrac{\left(ep^{0.5} \cdot \cos(\theta 3) - n \cdot T2\right)}{\left(ep^{0.5} \cdot \cos(\theta 3) + n \cdot T2\right)}$:

> $r23 := \dfrac{\left(T2 - ep^{0.5} \cdot T3\right)}{\left(T2 + ep^{0.5} \cdot T3\right)}$:

R is the total reflectivity at the thin film.

> $R1 := \dfrac{(r12 + r23 \cdot \exp(-2 \cdot k \cdot d))}{(1 + r12 \cdot r23 \cdot \exp(-2 \cdot k \cdot d))}$:

> $R := R1 \cdot (conjugate(R1))$:

Ta is the percentage of light entering the prism.

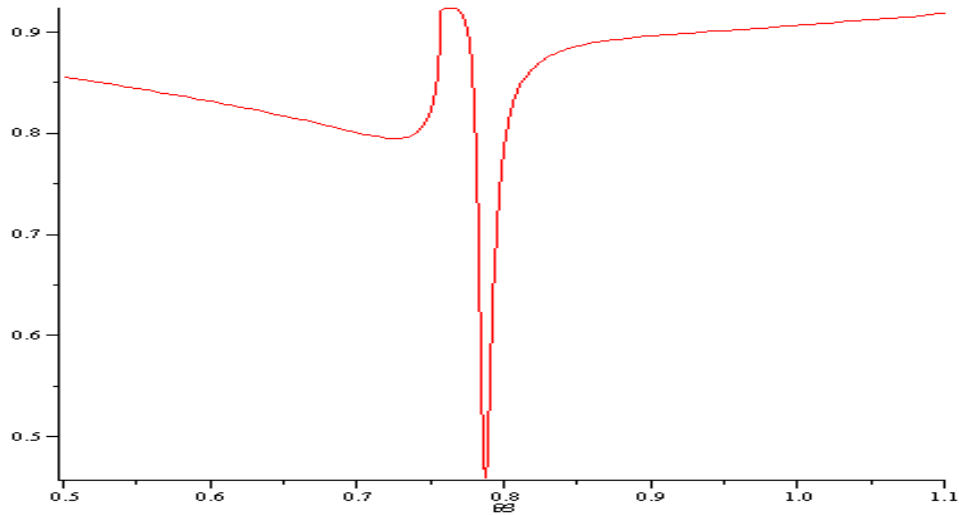Tc is the percentage of light exiting the prism.

> $Ta := 1 - \left(\dfrac{\cos(\theta 2) - n \cdot \cos(\theta 1)}{(\cos(\theta 2) + n \cdot \cos(\theta 1))}\right)^2$:

> $Tc := 1 - \left(\dfrac{n \cdot \cos(\theta 1) - \cos(\theta 2)}{(n \cdot \cos(\theta 1) + \cos(\theta 2))}\right)^2$:

Rmain is the total reflected light exiting the prism.

> $Rmain := Tc \cdot R \cdot Ta :$

> $plot(Rmain, \theta3 = .5 ..1.1)$

thetap is the plasmon absorption angle.

> $thetap := \arcsin\left(\dfrac{\left(\dfrac{ep}{ep + 1}\right)^{\frac{1}{2}}}{n}\right)$

thetap := $0.7835216298 + 0.0006220365248\, I$

Below are the commands that export the theoretical model into excel.

s creates a sequence of data points of Rmain from incident angle of .5 radians to

1.1 radians in .003 incriments.

m converts s to a matrix

mm converts the matrix from a row matrix to a column matrix

A converts the matrix to an array, so it can be exported

after opening an AddIn in Excel, with(ExcelTools) opens the Maple package

needed

Export sends the data to Excel.   You can send the data to any file, sheet, or cell

name you want, but the Excel file must be closed when you export and you have to paste

the column of data into another file to work with it.

> $s := \left[seq \left(\mathrm{Re}(evalf(Rmain)), \theta3 = .5 ..1.1, \right. \right.$
  $\left. \left. .003 \right) \right] :$

> $m := convert(s, Matrix)$

$$m := \begin{bmatrix} \textit{1 x 201 Matrix} \\ \textit{Data Type: anything} \\ \textit{Storage: rectangular} \\ \textit{Order: Fortran\_order} \end{bmatrix}$$

> $with(LinearAlgebra) :$

> $mm := Transpose(m)$

$$mm := \begin{bmatrix} \textit{201 x 1 Matrix} \\ \textit{Data Type: anything} \\ \textit{Storage: rectangular} \\ \textit{Order: Fortran\_order} \end{bmatrix}$$

> $A := convert(mm, Array)$

$$A := \begin{bmatrix} \textit{1..201 x 1..1 Array} \\ \textit{Data Type: anything} \\ \textit{Storage: rectangular} \\ \textit{Order: Fortran\_order} \end{bmatrix}$$

> $with(\textit{ExcelTools})$: